The Meteoritical Society

Meteoritics & Planetary Science 1–22 (2024)
doi: 10.1111/maps.14152

Icy ocean worlds, plumes, and tasting the water

M. J. BURCHELL* and P. J. WOZNIAKIEWICZ*

Centre for Astrophysics and Planetary Science, School of Physics and Astronomy, University of Kent, Kent, UK
*Correspondence
M. J. Burchell and P. J. Wozniakiewicz, Centre for Astrophysics and Planetary Science, School of Physics and Astronomy, University of Kent, Canterbury, Kent CT2 7NH, UK.
Email: m.j.burchell@kent.ac.uk and p.j.wozniakiewicz@kent.ac.uk

(*Received 28 October 2022; revision accepted 12 February 2024*)

Abstract–This paper considers how space missions that fly through the plumes known, or suspected, to erupt naturally from some icy ocean worlds (IOW), such as Enceladus, or that aim to intercept icy ejecta from impact cratering processes on such bodies can sample the water and ice within the plumes. The mechanics of how grains (either in the plumes or the ejecta) would interact with a passing spacecraft (i.e., impact speeds, shock pressures, etc.) are introduced. The impact speeds are estimated and vary with both the mass of the IOW and the orbital parameters of a space mission. This can lead to large differences in impact speeds (and hence collection methods) at bodies such as Enceladus and Europa. The implications of these different impact speeds (a few hundred m s^{-1} to several km s^{-1}, and even greater than 10 km s^{-1}) for the collection of organic materials from the plumes are shown to be significant.

INTRODUCTION: ICY OCEAN WORLDS

Previous Missions

The icy satellites of the outer planets are bodies of increasing interest to planetary science. Following the break-through work of the Galileo mission at Europa, several of the satellites of Jupiter and Saturn (Figure 1) are now known/suspected to have global oceans of liquid water underneath their icy exteriors, with a solid core in the center of the body, for example, Europa (e.g., Carr et al., 1998; Jia et al., 2018; Khurana et al., 1998; Kivelson et al., 2000; Pappalardo et al., 1999; Sparks et al., 2016; Zimmer et al., 2000), Ganymede (e.g., Kivelson et al., 2002), Callisto (e.g., Khurana et al., 1998; Zimmer et al., 2000), Enceladus (Čadek et al., 2016; Hemingway et al., 2018; Iess et al., 2014; Nimmo et al., 2007; Postberg et al., 2008, 2009; Schenk et al., 2018; Thomas et al., 2016; Waite et al., 2006), and Titan (e.g., Béghin et al., 2012; Hemingway et al., 2013; Lorenz et al., 2008).

Furthermore, as pointed out by many (e.g., Hendrix et al., 2019), there are also other bodies that may contain significant volumes of internal liquid water, including Triton (a Moon of Neptune). The combined quantities of water for these bodies are likely more than 50× that on Earth (Hall, 2015), with Europa, Ganymede, and Callisto each likely to contain more liquid water than the Earth's oceans. However, by far the dominant location of liquid water may be Titan, whose liquid water content might dwarf that of Earth. However, details of the interior of Titan are still uncertain, so estimates of the water content are not well constrained (e.g., see Soderlund et al., 2020, for a discussion). Thus, precise measurements of the quantities of liquid water in these bodies require a more detailed knowledge of their interior structure and properties, as well as those of the other possible water-rich bodies such as Pluto, the Saturnian moon Dione, and the Uranian moons, where knowledge is so sparse we can currently only speculate.

The various methods leading to the deduction of an internal water layer with a solid core (i.e., moment of

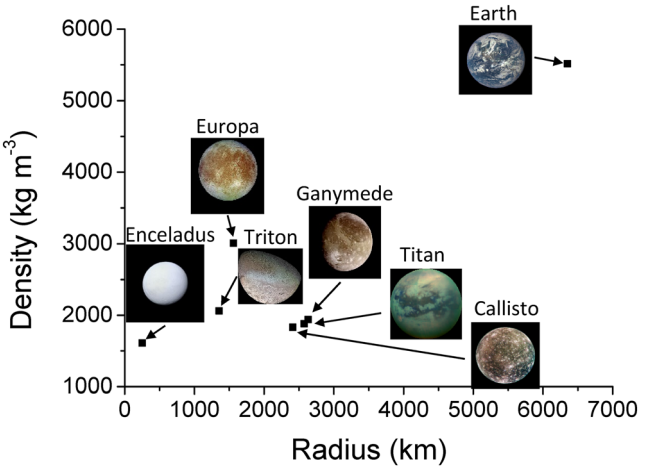

FIGURE 1. Sizes and densities of potential icy ocean worlds, compared to the Earth (image source: NASA).

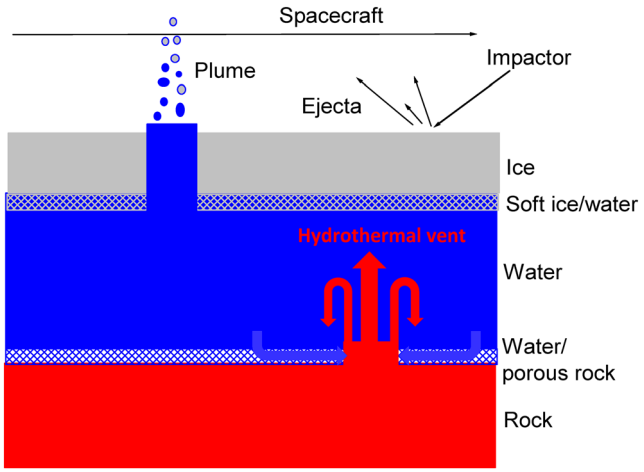

FIGURE 2. Schematic of the tri-layered structure of an icy ocean world. A solid central core (rocky here) has a water layer above it with an ice layer above that at the surface. At each of the internal boundaries, there may be a thinner mixed layer (e.g., water mixed with porous rock above the core and soft/slushy ice mixed with water beneath the surface ice). The core/water boundary may be crossed by a hot hydrothermal vent, or similar, releasing mineral-rich hot liquids/gases into the ocean. Similarly, the surface ice may be breached by plumes, which ejecta water into space above the body.

inertia, magnetic induction, geodesy, surface features, etc.) are summarized in a review by Nimmo and Pappalardo (2016). In addition to the bodies around Jupiter and Saturn, as stated, it is also possible that other bodies such as the Neptunian satellite Triton (e.g., Gaeman et al., 2012; Hussmann et al., 2006) and the minor body Pluto (e.g., Bierson et al., 2020; Nimmo et al., 2016) may also have similar tri-layered structures (Figure 2). Furthermore, other bodies may also contain significant amounts of liquid water in their interior. For example, Ceres is now thought to contain sufficient brine-rich water in its interior that, in some respects, it is now more akin to an icy satellite than an asteroid (e.g., for a review, see Castillo-Rogez et al., 2020).

This tri-layered structure is not only of interest in its own right, but the presence of liquid water also makes these bodies of particular interest for astrobiology. The liquid water in the oceans, with benign temperatures and pressures, plus potential sources of heat and chemicals at putative hydrothermal vents on the ocean floor/surface of the interior core (e.g., Hsu et al., 2015; Lowell & DuBose, 2005), provide the flux of energy and the bio-essential elements needed for a potentially viable habitat (e.g., see Hand et al., 2020; Vance et al., 2007).

Although, as indicated, there are several measurements indicating the presence of the internal oceans on each of Ganymede, Callisto, Europa, Enceladus, and Titan, the internal structures of the various icy ocean worlds (IOWs) are still not well constrained, and, for example, the NASA Roadmap to Ocean Worlds (Hendrix et al., 2019) lists the determination of the thickness of the ice shells and depths of the internal oceans as a major objective (e.g., see Hemingway et al., 2018, for a review of the estimates of ice shell thickness at Enceladus and Hemingway & Mittal, 2019, for a more recent, up-dated estimate of the thickness). The overall size and density of each of the main candidate worlds are, however, known and shown in Figure 1.

There are thus several distinct drivers for research into the IOWs. While their surfaces have been imaged, a more detailed study is needed along with the measurements of their interiors. Addressing this requires scientific investigation on not just a wide variety of size scales and variety of depths below the surface of the bodies, but also via the bringing together of multiple disciplines (planetology, chemistry, mineralogy, biology, etc.).

The outer planets have had relatively few visits by space missions: The grand tour Voyager missions (Voyager I to Jupiter and Saturn and then exited the solar system, and Voyager II, which flew past Jupiter, Saturn, Neptune, and Uranus and then also exited the solar system), the Galileo and the current Juno missions (to Jupiter), the Cassini mission (to Saturn), and the New Horizons mission (to Pluto and Kuiper Belt). Given that Neptune and Uranus have only been visited once (via a flyby), the inventory of IOWs and their properties should be considered incomplete, and the amount of liquid water in the outer solar system will in future undoubtedly be revised significantly upwards. For example, the recent Decadal Survey, 2023–2032 (National Academies of Sciences, Engineering, and Medicine, 2022), placed a Uranus mission as the highest priority for a new Flagship-class mission. Such a mission to an ice giant like

Uranus would undoubtedly greatly extend our knowledge of the planet's satellites and their interiors, including any water content.

As well as discovering and characterizing the various IOWs, one previous mission (Cassini) has already sampled the water they contain. This was possible because, in the case of Enceladus, it was discovered that plumes of water erupt from vents in the icy surface (e.g., Hansen et al., 2006; Porco et al., 2006; Waite et al., 2006). The mechanism behind these plumes is discussed, for example, in Goldstein et al. (2018), and Spencer et al. (2018). As well as vapor, the plumes also contained discrete dust grains, which triggered the Cassini High Rate Dust Detector (Spahn et al., 2006). Fortunately, the Cassini spacecraft also carried a Cosmic Dust Analyzer (CDA), which used impact ionization of sub-micron and micron-sized grains to determine the composition of particles it encountered (Srama et al., 2004). During flybys of Enceladus, which took Cassini through the plumes, CDA revealed not only that the plumes contained ice grains and various salts and minerals (e.g., Hillier et al., 2007; Postberg et al., 2008, 2009, 2011), but also that there were both low and high mass organics present within the plumes (Khawaja et al., 2019; Postberg et al., 2018 respectively), as well as sodium phosphates (Postberg et al., 2023).

Present and Future Missions

A wide range of space mission types (flybys, orbiters, or landers) can potentially study any target body. Subclasses of missions are also possible. For example, in the case of landers, it can be a soft lander on the surface or a penetrometer that reaches down up to 10 m under the surface. Future missions to IOWs will thus include a combination of flybys, orbiters, and landers to better characterize these bodies.

One such currently active mission is NASA's Juno mission to Jupiter, which arrived at Jupiter in 2016. Although primarily a mission to study Jupiter itself, the spacecraft also made a flyby of Ganymede in June 2021, passing within 1000 km, and a closer flyby of Europa in September 2022, at an altitude of 352 km. The data from these flybys has provided high-resolution images of the surfaces and will allow us to probe the near subsurface with microwave radar.

The next NASA mission to Jupiter, the Europa Clipper mission, will study Europa in detail. Europa Clipper is projected to launch in October 2024 and arrive at Jupiter in April 2030. It will orbit Jupiter (rather than Europa itself) and make repeated low altitude passes around Europa. The mission, however, shows the difficulties in planning a detailed visit to a distant body, in that while plumes from the interior are suspected and have been reported (Sparks et al., 2016), they are not confirmed, and even if present may be sporadic or weak. A detailed characterization of Europa is therefore the mission goal, which will include details of the interior ocean, but the Europa Clipper is not a life-detection mission per se. It does, however, carry a dust impact ionization detector, SUDA (Goode et al., 2023; Kempf et al., 2014), which could observe plume contents if present, but which will primarily observe dust particles knocked off the European surface by micrometeorite impacts. Given that these ejecta are mostly low speed, the encounter speed with the Europa Clipper will be determined by the spacecraft motion past Europa, with a typical speed of a few km s^{-1}. This impact speed is just inside the impact ionization regime, and likely to provide signals from large organic molecular fragments from the dust grains, although speeds of 4–6 km s^{-1} are recommended for best results for organic materials in ice (see Klenner et al., 2020 and discussion below in Sub-Micrometre Particles section).

The ESA Juice mission to Jupiter (launched in April 2023 and due to arrive at Jupiter in 2031) will not only orbit Jupiter but will also focus on the IOWs Europa, Ganymede, and Callisto (Grasset et al., 2013). Indeed, it is planned to enter orbit around Ganymede in 2034, becoming the first spacecraft to orbit an IOW. The initial orbit at Ganymede will be highly elliptical ($200 \times 10{,}000$ km), but this will then be adjusted to a circular orbit at initially 5000 km and subsequently lower altitude (e.g., 500 km). Its instrument payload includes precision gravity field measurement and radar (for near-surface studies of the icy satellites up to 9 km in depth), as well as surface mapping and composition-determining instruments.

For future missions to an already studied IOW such as Enceladus, where plumes are confirmed and fairly well characterized physically, other options exist, including collecting material from the plume (see, for example, mission proposals by MacKenzie et al., 2021; Mitri et al., 2018; Mousis et al., 2022; Reh et al., 2016). When considering sample collection from the plume, it should also be acknowledged that, as well as passing through the plume, a separate lander can access the collected material that has fallen from the plume over time (a process that can concentrate the plume material). Landers, however, add complexity to any mission and increase the planetary protection issues (see below). Nevertheless, the Enceladus Orbilander concept was recommended by the National Academies Decadal Strategy for Planetary Science and Astrobiology 2023–2032 as the second highest new Flagship mission priority (National Academies of Sciences, Engineering, and Medicine, 2022). Such a mission would start with a 1½ year orbital mission of Enceladus (collecting plume samples and characterizing the surface), followed by a landing and a subsequent 2 year surface science mission. It would deploy a variety

of instruments to try to answer a wide range of scientific questions regarding Enceladus (see MacKenzie et al., 2021, 2022).

For IOWs, missions are, however, made more complicated by their status as potential habitats for life, that is, planetary protection protocols (PPP) apply (see COSPAR, 2021). These cover not only the risk to the Earth from returned samples potentially introducing alien material here, but also the hazard to the original environment from any material potentially introduced by the mission. The perceived risk increases, and the complexity and restrictions are accordingly imposed, as the categories progress from I to V. Not all the IOWs are in the same PPP category in the COSPAR scheme. Callisto, Ganymede, Titan, Pluto, and Triton are all possible category II (although a self-declaration of this is deemed insufficient and must be accompanied by a risk analysis). Missions to Enceladus and Europa are category III for flybys and orbiters, and category IV for landers. Earth return missions are category V. Even within the general categories III, IV, and V, the special status of Enceladus and Europa means they are subject to specific extra discussion (section 10 within the PPP). A full future exploration program would envisage multiple visits to each IOW, and general techniques to study icy satellites and their internal oceans are summarized in Taubner et al. (2020), for example. Clearly, given the cost and duration of individual missions, this will be a multi-decade activity involving several generations of planetary scientists. Decisions on priorities therefore have to be made, and an early one (akin to the Mars post-Viking era) is simply as to whether a mission should have astrobiology as its focus or general environmental characterization. The issue is, however, different to Mars, in that, while in both cases there is no obvious sign of life, on the IOWs there is abundant liquid water. Further, in the case of Enceladus, there is clear evidence from Cassini CDA data that the ocean contains complex organic molecules.

The level of detail needed to characterize the interior of an IOW sufficiently to confirm the presence of an interior ocean and to find the thickness of the surface ice and liquid water layers may well require not just flybys while in orbit around the parent planet, but also orbiting the IOW itself at low altitude. So far, the only planetary satellite to be orbited by a spacecraft is the Earth's moon, but the ESA JUICE mission in the 2030s will not only initially orbit Jupiter but, as already stated, later in its mission will enter orbit around Ganymede (Grasset et al., 2013). The JUICE mission profile includes lengthy periods in circular orbits at low altitude to help map details of the body with greatest resolution, with no area preferred for special treatment. However, at Enceladus, the plumes are clearly a site of special interest, and the proposed NASA Enceladus Orbilander mission (MacKenzie et al., 2021) therefore proposes to use elliptical orbits of that body, allowing very low altitude passes at periapsis through the plumes. It is also possible (as already stated) that the continual impact flux on the surface can produce ejecta, which, for impacts on organic-rich ices, can contain detectable organic material (e.g., Burchell, Bowden, et al., 2014), which could be sampled by a passing spacecraft. Similarly, heavy ion bombardment of the icy surfaces could liberate (via sputtering) intact organic molecules, which could again be sampled by a passing spacecraft (e.g., Anders et al., 2020; Johnson & Sundqvist, 2018).

Given that the water inside Enceladus is accessible via its plumes, the potential for plumes at other IOWs also arises. There is also some evidence that Europa possibly has plumes that are taken as arising from an internal ocean (e.g., Jia et al., 2018; Roth et al., 2014; Sparks et al., 2016), although it has also been suggested that any plumes at Europa may arise from eruptions from trapped, subsurface lakes within the ice surface layer (see Lesage et al., 2022, and references therein). Indeed, the first plumes on an icy body were observed at Triton by Voyager II (Soderblom et al., 1990). It is not clear if the plumes at Triton originate from an internal ocean, or, are (near-)surface phenomena driven by solar radiance; however, renewed interest in their origin (e.g., Hofgartner et al., 2022) has led to calls for a new mission to the Neptunian system. In all cases, the attraction is that any water can be sampled by flying through the plumes, greatly simplifying mission planning and complexity, and reducing the risks of contamination of the surface ice or internal ocean. Some planetary protection risks do still arise, if the spacecraft (an orbiter or a single/multiple fly past mission) were to lose control and impact the surface, there is still a risk of contamination, particularly if it were to strike a vent at the base of a plume. Nevertheless, it is possible to reasonably plan outbound missions to bodies such as the IOWs, both in terms of cost and planetary protection, including examples relating to Enceladus (e.g., MacKenzie et al., 2021, 2022; Mitri et al., 2018; Reh et al., 2016) and Europa (e.g., Hand et al., 2017). Furthermore, as well as selecting a target body, the question then becomes, what sort of mission?

Flying through a plume, and in effect tasting the water drop by drop during the passage, is an effective way to collect data, without the need for a lander. If we ignore the issues of how to characterize the target body itself (e.g., surface ice layer thickness, core size and composition, etc., which is a multi-scale and multi-disciplinary problem), the key questions are how does one sample a plume, and what might you find? This raises, in turn, the question of how the sampling method might influence the results of any subsequent analysis.

In the rest of this paper, we focus on the possibility of sampling the water in the plumes rising above the surfaces of some of these bodies, with an emphasis on the physical and technical challenges involved in such sampling.

PLUME SAMPLING APPROACHES

There are several ways to fly through a plume emitted from an IOW—by flying past the target body or by orbiting it (see Figure 3). The fly past option could involve a single flyby of an isolated icy body (e.g., New Horizons at Pluto; see Stern et al., 2015) or, if it were a Moon, a flyby of its parent planet observing the IOW's along the way (e.g., as in the cases of Voyagers I and II). Equally, for Moons, multiple flybys are possible if the spacecraft were in orbit around the parent planet (Galileo and Juno at Jupiter, and Cassini at Saturn). In all cases, the flyby speed of the IOW will be high. A single flyby while heading past into deep space will be at high speed (e.g., ~10 and 16 km s^{-1} for Voyager II at Jupiter and Saturn, respectively, and ~14 km s^{-1} for New Horizons at Pluto, Stern et al., 2018). Flybys, while in a planetary orbit, will depend on the particular mission profile and can vary from flyby to flyby, even for the same target body (e.g., Cassini at Enceladus had encounter speeds in the range of approximately 6–18 km s^{-1}; see Lorenz & Burk, 2018). With appropriate mission planning, it might be possible to lower the Enceladus flyby speed to ~3 km s^{-1} (Tsou et al., 2012).

As well as the three options to fly through the plume, as already stated, a fourth mission scenario exists to sample plume material, namely a lander. This could access the collected material that has fallen from the plume over time (a process that can concentrate the plume material). However, much of the material of interest will be sensitive to radiation damage and environmental effects, so simply scooping it off the surface may not be sufficient. Conveniently, fresh material will continually rain down from the plume for immediate collection. Such collection involves landing underneath the plume so that the plume material falls continually as a shower of frozen material onto the lander. This "snow" of material is still relatively fresh (having ascended and then descended again) and arrives as a continual flux. The material will include the full size range of ejected material, whereas an orbiter or flyby will be limited by what size material reaches the altitude at which collection occurs (see later discussion). However, depending on the dynamics of the plume, there may well be size-sorting effects in the distribution of the material as it lands, so the location of such a lander relative to the source of the plume would be important. The "collection speed" would be determined by the in-fall speed of the material, which, in the absence of any appreciable atmosphere or retarding forces, would be determined by local gravity and the altitude at which descent starts. Descent of a particle from 1 (or 10) km, for example, would lead to speeds of order 15 (and 47) m s^{-1} at Enceladus and 51 (and 162) m s^{-1} on Europa. The peak altitude is determined by the emission speed at the base of the vent (assuming no further acceleration) and can be correlated with particle size. These effects were simulated for Enceladus, for example, by Southworth et al. (2019), which found that in some regions on the Enceladan surface, the influx rate can reach up to 0.1–1 mm year^{-1}. It is thus no surprise that it has been estimated that, over a given period, such a lander might well yield a significantly greater flux of plume material than that available via orbital collection, increasing the amount of collected material by several orders of magnitude compared to an orbiter or flyby mission (e.g., see Porco et al., 2017). There would, however, be significant PPP implications for such a mission. Further, if a mission solely comprised a lander, it would not be able to characterize the whole body, so it would likely be part of a multi-mission architecture or a single mission combining an orbiter and a lander, such as the NASA Enceladus Orbilander concept (see Enceladus Orbilander, 2021; MacKenzie et al., 2021, 2022).

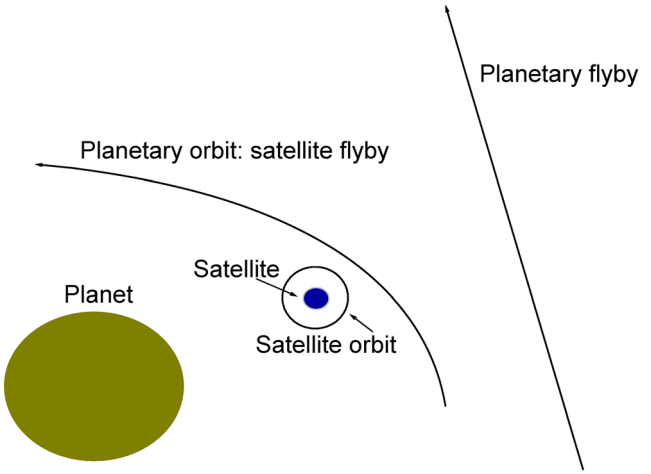

FIGURE 3. Schematic of orbital scenarios to visit an icy ocean world. A flyby of the parent body is one option (e.g., Voyager missions on their Grand Tour). Orbiting the planet and making a number of near flybys of the target satellite is a second option (e.g., Galileo or Cassini). Orbiting the target satellite itself is a third option.

Orbital Speeds

Orbiting the target body itself produces a speed and period that depend on both the individual IOW and the altitude of the orbit. For illustrative purposes, we assume an unpowered, gravitationally bound, circular or elliptical orbit (actual orbits will depend on the particular

mission profile and may well be highly elliptical). The true orbits will be perturbed by the presence of the large mass of the parent planet, requiring the solution of a three-body calculation, but the simple two-body calculation is used to provide an indication of the magnitude of speeds in the range of altitudes of interest (e.g., see Fantino et al., 2020). In the case of Enceladus, the combination of the large mass of the parent body and the low mass of Enceladus can lead to large orbital perturbations (e.g., Massarweh & Cappuccio, 2020; Russel & Lara, 2009), which will, in some mission scenarios, require active control on each orbit (e.g., Enceladus Orbilander, 2021).

In Figures 4 and 5, the resultant orbital speeds and periods are shown versus altitude for the main candidate IOWs. The speeds (Figure 4a) fall into three groups depending on IOW mass (see Figure 1): (i) At Enceladus, the speed is approximately 0.1–0.2 km s^{-1}, (ii) at Triton, it is around 1 km s^{-1} and is just below 1.5 km s^{-1} at Europa, and (iii) for the more massive Callisto, Titan, and Ganymede, it is 1.5–2 km s^{-1}.

If elliptical orbits are used (as likely in reality, to permit low altitude passes through a suspected plume region, combined with extended coverage of the whole body during the rest of the orbit to permit characterization of the whole surface), the spacecraft speed will vary around the orbit. Here, the key speed is that which occurs during the transit of the plume. This would occur at periapsis, which would be low (given the inverse correlation of particle number in the plume with altitude) to maximize the capture efficiency of the plume contents. If we assume an altitude at apoapsis of 1000 km (a typical value for Enceladus mission planning, for example), then at periapsis, the increase in spacecraft speed relative to that for a circular orbit at the same altitude is shown in Figure 4b. It can be seen that for most IOWs, the increase in speed is modest, even at low periapsis altitudes. In the worst case (Enceladus), even with the altitude at periapsis well below 100 km, the increase in impact speed will only be of order 35%–40%. These results change slightly with the choice of apoapsis within a reasonable range, but the general result stays the same, the impact speeds at periapsis (i.e., when plume sampling will occur) are roughly as for a circular orbit at that altitude.

This variation in spacecraft speed with the different IOWs and choice of orbit has consequences for mission planning, as the different speed regimes imply different shock pressures during impacts between the spacecraft and the discrete components of the plume. Note, in particular, that impact speeds in excess of a few km s^{-1} are often termed hypervelocity and involve shock pressures in the 10–100 s of GPa range for solid materials. Such impacts have significant consequences for materials concerned, involving

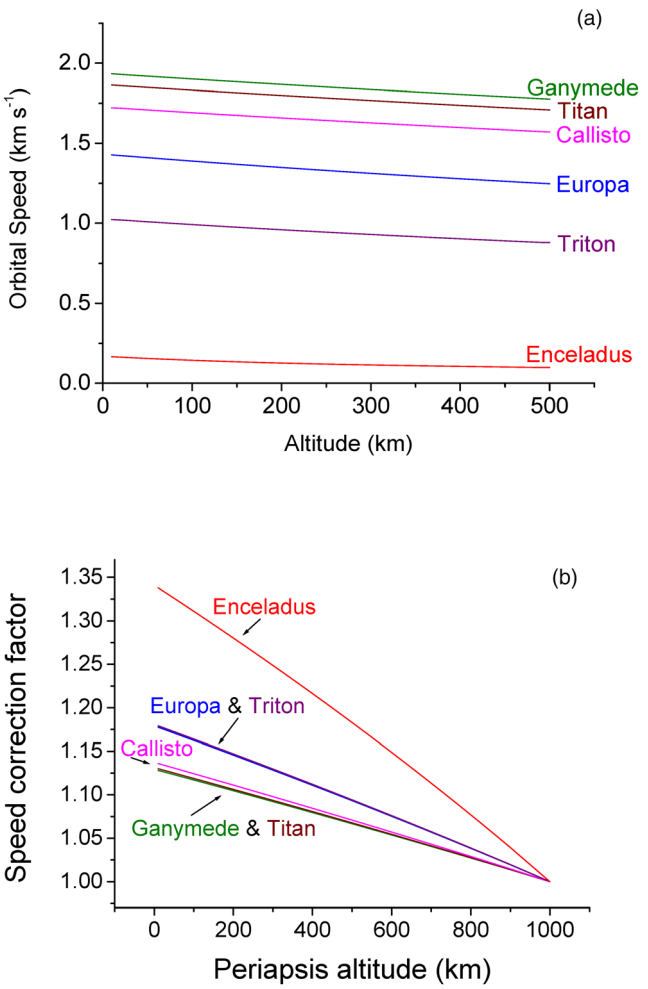

FIGURE 4. (a) Orbital speed versus altitude for circular orbits around the main candidate, icy ocean worlds. Orbital speeds are lowest at Enceladus due to its low mass. An earlier version of this figure (for just Enceladus and Europa) appears as fig. 4 in Traspas and Burchell (2021). (b) Correction factors adjusting the speed in (a) to give speed at periapsis, assuming an elliptical orbit with a periapsis altitude equal to the altitude in a circular orbit and an apoapsis altitude of 1000 km.

fracturing, heating, melting, partial vaporization, etc. Collecting macroscopic samples in such impacts and understanding their nature is a specialist discipline. Further, if low orbital speeds occur (e.g., as at Enceladus), although the impacts will not be hypervelocity, the motion of the material in the plume itself cannot be ignored and may make a significant contribution to the total impact speed and impact direction on the exposed spacecraft surface. While dust grain speeds in a plume will be lower than the gas speeds (estimated at up to 1 km s^{-1}), they may not be totally negligible for the low orbital speeds at Enceladus, for example, Degruyter and Manga (2011) estimate that large plume particles at Enceladus travel at up to 200 m s^{-1}, that is, comparable to the spacecraft speed.

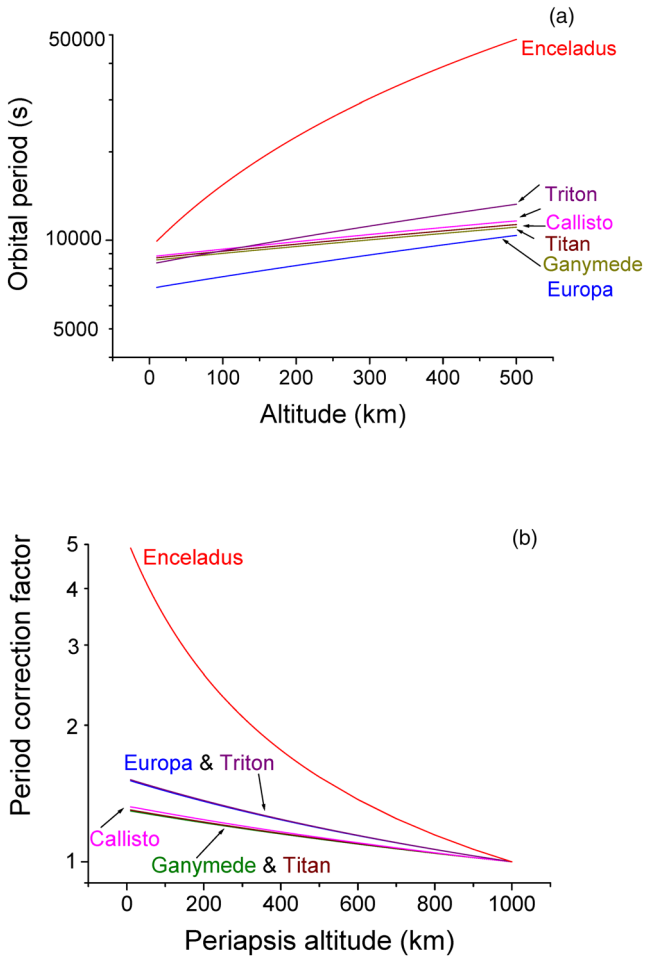

FIGURE 5. (a) Orbital period versus altitude for circular orbits. The periods are greatest at Enceladus due to its low density; they also rise fastest with altitude at Enceladus due to its small radius. (b) Correction factors for the periods in (a) assuming an elliptical orbit with a periapsis altitude equal to the altitude in a circular orbit and an apoapsis altitude of 1000 km.

Orbital Periods and Flux

The frequency of collection on an orbiting spacecraft depends on the period, and the total flux collected depends on the number of passages through the plume during the orbiting phase of the mission (again, period-dependent). The orbital periods (again assuming circular orbits for convenience) are thus shown in Figure 5a. It can be shown (see Appendix 1) that at low altitudes (or low to moderate altitudes for large parent bodies), the period for a gravitationally bound circular orbit around a body converges to a value given by $\sqrt{[3\pi/G\rho]}$. For worlds with similar densities, such as Ganymede, Callisto, Titan, and Triton, where the average of the various bulk densities is 1927 kg m^{-3}, this gives an orbital period of 8563 s, or 143 min. Hence, the curves for these IOWs in Figure 5a cluster together. That, at negligible altitude, Enceladus (9365 s) and Europa (6849 s) have greater/smaller periods in Figure 5a, reflects their lower/greater bulk densities shown in Figure 1 (illustrating the inverse dependence on density). The steep increase in period with altitude exhibited at Enceladus is a consequence of the small mass of that body. Similarly, the intermediate sizes of Europa and Triton mean that the orbital periods around these bodies rise faster with increasing altitude than they do for larger bodies such as Ganymede, Callisto, and Titan.

Orbital periods for non-circular orbits will depend on the nature of the orbit, with longer periods associated with larger semi-major axes. The increase in orbital period at the IOWs for elliptical orbits with an altitude at apoapsis of 1000 km versus circular orbits at a given periapsis altitude is shown in Figure 5b. In all cases, except Enceladus, the increase in orbital period is modest, even at low values of the periapsis altitude. Different choices of the apoapsis will alter the results slightly. At Enceladus, for example, halo orbits have been proposed for the Enceladus Orbilander (Enceladus Orbilander, 2021; MacKenzie et al., 2021, 2022; Orbilander, 2021) with periapsis altitude lower than 50 km and apoapsis altitude up to 1000 km, with an associated orbital period of around 12 h.

The captured flux from any mission is the combination of the flux intercepted in a single pass through the plume and the total number of passes. If the altitude of the pass changes, or the path through the plume, the orientation of the spacecraft, etc., then the intercepted flux from pass to pass through the plume can vary. Indeed, if the plume activity is not constant and uniform, the collected flux will again vary with each passage.

There are several models of plume contents versus altitude at Enceladus. For example, Tsou et al., 2012 (also see references therein) estimate that 150–350 kg s^{-1} is emitted in the Enceladan plumes. Note, however, that this total mass rate includes both vapor and dust grains. Based on analysis of Cassini data, Hansen et al. (2020) estimate that the rate of emission of water molecules is 300 kg s^{-1}, with an annual variation of <15%. Guzman et al. (2019) estimate that the dust content alone is emitted at a rate of 16 kg s^{-1}. This material spreads out as the plume rises, and at 80 km altitude, it is estimated by Tsou et al. (2012) to yield 1 ice grain per m^3. Such a low concentration has consequences in mission planning (e.g., MacKenzie et al., 2021; Mitri et al., 2018; Reh et al., 2016). Of the various possible encounter methods (Figure 3), a flyby of the parent planet permits only one opportunity for sampling. Even the method of orbiting the parent planet and occasionally passing close to the

target IOW offers only limited collection opportunities. For example, the Enceladan mission proposed by Tsou et al. (2012), only had 3–4 Enceladan flybys during an 8-month Saturnian system tour. A multi-year sojourn in the Saturnian system would increase the number of flyby opportunities, but there would also be other mission objectives competing for orbital trajectories past various other Saturnian satellites. By contrast, a temporary low altitude circular orbit of Enceladus would sample the plume typically every 11,000 s, that is, approximately once every 3 h (see Figure 5a), although it should be noted that Saturnian perturbations preclude a stable circular orbit at Enceladus (e.g., see Massarweh & Cappuccio, 2020).

The altitude of an encounter is critical and will need to be different at different bodies due to their different masses influencing the local escape velocity (e.g., 0.239 km s^{-1} for Enceladus vs. 2.025 km s^{-1} for Europa; see Southworth et al., 2015). At Europa, for example, Lorenz (2016) estimated that while 20 μm-sized objects could be lifted to the plume top at 200 km, larger 2 mm objects would be restricted to altitudes of just 2 km, with a total plume particle flux of 1.5×10^{-8} kg m^{-3} at 10 km altitude. By contrast, Southworth et al. (2015), indicate that the largest size grain that would be encountered at low altitude in a plume at Europa would be <90 μm, with grain size reducing to 30 μm at 15 km altitude. This size sorting of material with altitude within a plume will be just as critical as the number flux in determining how much material will be collected for analysis. The size difference between 20 μm and 2 mm implies a million times difference in mass, for example.

The width of a plume at a given altitude is also important in determining the collected mass. If we assume the spacecraft transits a near-vertical plume at normal incidence, the lateral spread of the plume will determine what fraction of the material lofted to that altitude will be collected. In his model, Lorenz (2016) assumed an Europan plume with a base vent up to 12 m in radius. The opening angle of the plume then determines its width versus altitude. By assuming an opening half angle of 30°, the width of the plume at any altitude is only just greater than the sum of the altitude and vent width. More collimated plumes can be assumed, however, as perhaps is the case at Enceladus. At Enceladus, Guzman et al. (2019) predict that with an active collector area of 1 m^2, a single passage through a plume at an altitude of 20–60 km, will collect some 1500 μg of material.

Various models can be used to predict the possible organic and microbial contents of an Enceladan plume. For example, Porco et al. (2017) predict that it is possible that a single plume passage at 50 km altitude could collect about 100 cells with a collector area of 0.04 m^2. However, as stated, not all plume models predict large grains of interest at significant altitudes. For example, Kotlarz et al. (2020) predict that, in their model for Enceladus, 2 μm-sized microorganisms would be lofted to, at most, just 1 km altitude. The difference compared to other models lays in the assumptions concerning the initial velocity of the grains, driven by gas pressure (i.e., Guzman et al., 2019) or equating thermal and kinetic energies (Kotlarz et al., 2020).

Peak Pressures

Impact-induced shock pressures in materials can be calculated using the planar impact approximation (PIA; e.g., Ahrens & Johnson, 1995; Melosh, 2013), and values versus impact speed are given in Figure 6 for a range of materials impacting aluminum (a typical material used as a target). In Figure 6, we use impactors of ice, polymethyl methacrylate (PMMA, as a proxy for complex organic material), and olivine (as a typical mineral). We have previously used PMMA as a standard proxy for low-density organic materials in hypervelocity impact experiments (e.g., Burchell & Armes, 2011), and are currently developing a range of other organic projectiles, for example polystyrene (Burchell & Harriss, 2020), anthracene (Chan et al., 2021), and phenanthrene (Chan et al., 2023), to widen the study of such materials in impact studies.

The PIA is based upon equating shock pressures in the projectile and target materials. These are found by solving the shock Hugoniot relations in both materials, assuming a linear wave speed relationship between shock speed (U) and particle speed (u), holds in each. This is of the form $U = C + Su$. Thus, solving the PIA requires the linear wave speed coefficients (C and S) for each material in the impact (projectile and target), and the values used here are given in Table 1 (along with the projectile and target densities, which are also required). The C and S values depend on shock speed, and at the lower end of the impact speed range considered here, values may differ slightly from those given. However, varying these parameters for olivine, for example, changes the peak shock pressure by at most 10% at the lowest speeds.

Looking at Figure 6, it can be seen that in general, at speeds just below 1 km s^{-1}, impacts on solid surfaces produce peak shock pressures around or below 1 GPa for low-density impactors, and of a few GPa for olivine. The peak shock pressure then rises with increasing impact speed, and at 5 km s^{-1}, it approaches 10 GPa for low-density impactors and some 60 GPa for olivine. At 10 km s^{-1}, peak pressures are around 100 GPa for the low-density impactors, and are already several hundred GPa for olivine. To understand how typical these values are, Burchell and Kearsley (2009) calculated peak

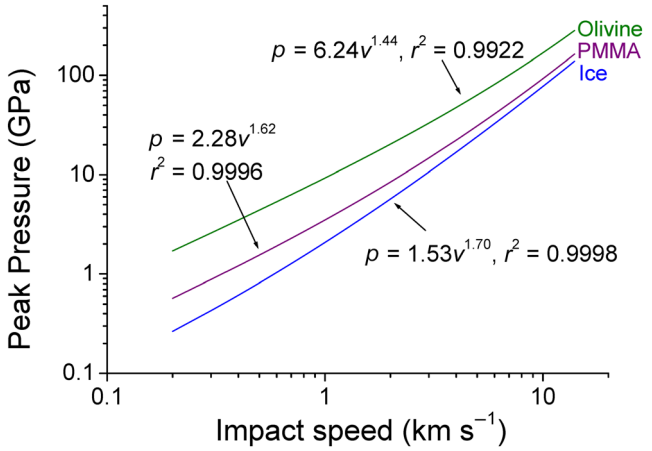

FIGURE 6. Peak shock pressures for ice, PMMA, and olivine impacting aluminum at a range of speeds (normal incidence is assumed). Pressures were calculated using the planar impact approximation with coefficients from Table 1. The fits shown use pressure P in GPa and impact speed v in km s^{-1}.

TABLE 1. Values required for use in the planar impact approximation (PIA). C and S are the coefficients in the linear wave speed relation of each material, and ρ is the density.

Material	Density (kg m^{-3})	C (m s^{-1})	S	Reference
Aluminum	2750	5300	1.37	Melosh (2013)
Ice	915	1317	1.526	Melosh (2013)
PMMA	1186	2766	1.365	Jordan et al. (2016)
Olivine	3246	6000	0.88	Ahrens and Johnson (1995)
Molybdenum	10,208	5140	1.25	Ahrens and Johnson (1995)

pressures for a range of minerals (anorthosite, augite, basalt, dunite, olivine, and spinel) impacting aluminum at a range of impact speeds. The increase in peak pressure with impact speed was similar to that found here. Also, at 2 km s^{-1}, peak shock pressures ranged from 12 to 18 GPa (i.e., ±20% around the mean value of 15 GPa).

The peak shock pressure also changes (albeit more modestly) if the target material is altered. For example, using a variety of targets in place of aluminum, such as gold, indium, silver, and copper, only changed the calculated shock pressure for impacts of ice at 1.5 km s^{-1} by ±0.35 GPa around a mean value of 3.8 GPa, that is, ±9% (see Traspas & Burchell, 2021). Similarly, at 2 km s^{-1}, impacts of an organic such as PMMA on the same range of target materials generate peak shock pressures ranging from 8.5 to 11.3 GPa (i.e., ±14%); see New et al. (2020). Thus, a scale can be set for impact shock pressures at relevant speeds, and can be seen to be more dependent on impactor type (lowest for ice, intermediate for organics, and highest for minerals) than target material.

IMPACT SHOCK-INDUCED CHANGES TO IMPACTORS

These shock pressures have consequences for the collection of plume material by a passing spacecraft. Material response changes dramatically over these impact speed/pressure ranges. In low-speed impacts (below a few hundred m s^{-1}), projectiles may rebound from a solid target. As speed (and shock pressure) increases, projectiles become embedded in the target as solid lumps. Between 0.5 and 1 km s^{-1}, the projectiles start to break up during the impact and leave smaller fragments in the crater, which now forms in the target. Above a few km s^{-1}, the projectile fragments are heated during the impact process, and form melt, lining the impact crater. At higher speeds, increasing amounts of the impactor are vaporized and lost from the impact site.

Sub-Micrometer Particles

Two projectile size regimes can be considered, above and below a few micrometers. For impactors a few micrometers or less in size, impact speeds of a few km s^{-1} or above are sufficient to vaporize a significant amount of the impactor. As well as being in a vapor, some of the material is also ionized, forming a so-called "impact plasma" at the impact site. If an electric field is applied, the charge can be separated and measured on collectors. Such impact ionization detectors (with metal targets) have long being used in space to measure the flux of <μm particles along with their mass (which is a function of the ionization signal and impact speed). However, if the electric field above the target is strong (accelerating the ions away from the target), followed by a longer region of low field in which the accelerated ions effectively drift to the collector, then a time-of-flight mass spectrometer can be built to determine the m/z values of the ions in the plasma. This is the principle of the CDA detector on Cassini (Srama et al., 2004).

However, there are significant impact speed effects in the creation of the impact plasmas. It has long been noted that the total charge recorded in impact ionization experiments depends on $m^{\alpha}v^{\beta}$ (impactor mass m and speed v), where $\alpha \sim 1$ but β ranges from around 3–5 for different metal projectiles impacting metal targets (Burchell et al., 1999; Dalmann et al., 1977). Of interest here is that Burchell et al. (1996) showed that this was also true for metal projectiles impacting ice targets (as an analog for ice particles striking a metal target), and

Goldsworthy et al. (2002, 2003) showed that this also applied to mineral and organic projectiles striking metal targets.

This speed dependence also influences the time-of-flight mass spectra arising from such impacts, as noted by Drapatz and Michel (1974), Dalmann et al. (1977), Kissel and Krueger (1987), and Ratcliff et al. (1997), and shown for mineral and organic impactors by, for example, Goldsworthy et al. (2002, 2003), Srama et al. (2009), Burchell and Armes (2011), Mellado et al. (2011), Hillier et al. (2012, 2014), and Fiege et al. (2014). At speeds of a few km s^{-1}, ionization and some bond scission occur, leaving large mass fragments with more peaks in the mass spectra appearing by about 5 km s^{-1}. As speed increases above ~10 km s^{-1}, more and more bonds break, with more detailed lower mass fragments emerging. Finally, above 20 or 25 km s^{-1} or so, the spectra show stronger elemental lines as the energy released into the projectile is sufficient to break most bonds. It is, however, possible to distinguish different organics from each other, even at modest speed (e.g., Burchell & Armes, 2011; Klenner et al., 2020). This is reviewed for organic impactors in Fielding et al. (2015).

Although it has long been shown that impacts on ice can produce impact ionization (e.g., Burchell et al., 1996), traditionally, it has been difficult to electrostatically accelerate small ice grains themselves. However, recently it has shown that it is possible to charge and accelerate (doped) 800 nm water ice grains at speeds up to 4.2 km s^{-1} (Burke et al., 2023). It is thus now possible to start directly studying in the laboratory water ice impact ionization spectra. Higher speeds are still needed, however, to see how the spectra evolve versus impact speed. What has been shown already by Burke et al. (2023) is that, for ice impacts on multi-channel ion plate targets at 2 km s^{-1}, there are no ionization mass spectra detected. However, at 2.7 km s^{-1}, a series of proton-water clusters are visible in impact ionization spectra, and the higher mass peaks disappear as impact speeds increase to 4.2 km s^{-1}. Furthermore, at 3 km s^{-1}, mass spectra can be obtained for amino acids added to the ice projectiles. This suggests a critical energy density is reached just above 2 km s^{-1}, which may be crucial for low encounter speed missions. For higher speeds (e.g., flybys), the way the characteristic amino acid mass spectra evolve with impact speed still remains to be elucidated.

Meanwhile, it is possible to use pulsed laser irradiation of doped liquid water to simulate impact ionization. This is shown, for example, by Klenner et al. (2019), who obtained mass spectra highly dependent on equivalent impact speed. Subsequently, Klenner et al. (2020) found that with an understanding of the dissociation chemistry of the organics in the presence of salts, it was possible to identify amino acids and fatty acids in the mass spectra (with differences noted in the cation and anion spectra, indicating that impact ionization detectors on spacecraft should be able to operate in both modes). How to understand the biosignatures in such mass spectra is also discussed, for example, in Jaramillo-Botero et al. (2021).

Care should be taken when using the PIA to find peak pressures for impacts involving particles below a μm in scale. This is because, although the PIA is supposed to be scale independent, some of the physical properties of materials change at high strain rates. For example, for some materials, strength properties change drastically (by many orders of magnitude) as strain rates exceed some 10^5 s^{-1} (Price, Kearsley, et al., 2013). Further, for very small particles, in-homogeneities, grain boundaries, etc., in the target metals can influence the outcomes of impact events. We therefore report the various thresholds above in terms of impact speed only, not pressure. This only emphasizes the need for experiments such as those by Burke et al. (2023).

The data from such impact ionization detectors therefore has to be carefully considered in terms of the impact speed and the chemistry of the impactor (which determine which bonds will preferentially break in a given impact). Nevertheless, current such detectors have high m/z resolution and can reveal the underlying chemistry of a wide range of organic impactors, provided the impact speed is above a few km s^{-1}.

Particles Larger than a Micrometer

For particles larger than a micrometer or so, the larger sizes mean that the classic sequence versus impact speed of rebound, sticking, and cratering (with initially projectile fragments embedded in the crater and then impact melt lining the crater) can be used to provide macroscopic samples for detailed analysis. The various thresholds for the transitions between these regimes are gradual rather than abrupt step functions. The sequence depends on the shock pressures, the elevated temperatures generated during the impact, and how soft the target is. The temperatures required for melting and vaporization also depend on the composition of the impactor.

This sequence of damage versus impact speed (shock pressure) was reported, for example, for soda lime glass impacting aluminum by Wozniakiewicz et al. (2018), who found that at 1 km s^{-1} (4 GPa), impactor rebound occurred. From 2 to 3 km s^{-1} (9–19 GPa), the projectile itself can be found in the crater, but with increasing fracturing at the higher speeds. Above 4 km s^{-1} (36 GPa), the impact crater is lined with melt, in which some fragments of partially melted projectile can be seen. Finally, above 6 km s^{-1} (61 GPa), only melt is seen in the

TABLE 2. Shock pressures thresholds various outcomes of impacts of ice (rebound, sticking, fragmentation, melting, and vaporization), with associated impact speeds for different target materials. These are for particles greater than a few μm in size.

	Pressure (GPa)		Mo target: Speed (km s^{-1})		Al target: Speed (km s^{-1})	
	Lower	Upper	Lower	Upper	Lower	Upper
Rebound	0.096	0.788	0.075	0.450	0.196	0.677
Sticking	0.287	2.07	0.200 (80%)	0.900 (20%)	0.374	1.20
Fragmentation	0.168	1.58	0.125	0.750	0.273	1.02
Melting	3	10	1.15	2.46	1.49	3.02
Vaporization	26	100	4.35	9.46	5.29	11.7

crater. Similarly, for salts impacting aluminum Fisher et al. (2021) (see Table 2 therein) reported finding impactor rebound at <0.5 km s^{-1} (<2.8 GPa), the appearance of impactor fragments in the craters at 0.5 to 1 km s^{-1} (2.8–6 GPa), signs of partial melting of fragments at 1–2 km s^{-1} (6–13.8 GPa), partial fragments in melt in some craters at 2–3 km s^{-1} (13.8–23 GPa), and at >5 km s^{-1} (>47.3 GPa) no fragments but extensive impact melting lining the craters. It should be noted that these results were from the impactors of a single composition. There is some evidence (Wozniakiewicz et al., 2012) that at 6 km s^{-1}, composite material impactors can behave differently to those of single grains, with more extensive melting occurring.

In general, there have been extensive studies of the collection of minerals in impact residues at speeds of up to 5 or 6 km s^{-1} (driven, for example, by the NASA Stardust sample return mission to comet Wild 2, for example, Burchell, Foster, et al., 2008; Burchell & Kearsley, 2009; Kearsley et al., 2007; Wozniakiewicz et al., 2012, 2014). However, there are relatively fewer studies of the fate of organics in impacts. One complication of trying to capture organic-rich materials is that impacts can drive increasing complexity via shock-induced chemistry. It has long been known that impacts can produce more complex molecules from simpler precursors (e.g., Bar-Nun et al., 1970; Blank et al., 2001; Peterson et al., 1997; Sugahara & Mimura, 2015; Takeuchi et al., 2020). Of particular interest here is that, it has previously been shown that impacts involving ices can drive chemistry (e.g., Bowden et al., 2009; Nna-Mvondo et al., 2008; Singh et al., 2022). Indeed, it has also been shown that amino acids can be produced in impacts onto ices (Martins et al., 2013). During collection from a plume, the reverse occurs, namely the ice strikes a target (rather than having impacts onto ice as in most experiments to date), but similar chemical processes should occur. This may well complicate flagging the origin of any organic molecules with the pre-impact source in that high-speed/high-pressure impacts may destroy or increase the chemical complexity present in the impacting material.

Careful calibration studies of such processes are thus required. For example, New et al. (2021) evaluated the survival of organic biomarkers in impacts on metals by firing ice particles (2–10 μm size range, doped with various organics) in the laboratory at metal targets. They used a light gas gun to achieve a speed range of 0.8–3 km s^{-1}, and found that the intact collection efficiency of these biomarkers varied with impact speed. Other methods of accelerating ice particles are also available, including Miller et al. (2022), who used electrospray technology to produce charged frozen droplets of water (size range 0.1–10 μm), which were then accelerated in a linear accelerator to speeds in the range 20–900 m s^{-1}. They reported that, as found for other projectiles, ice particles rebound from targets at the lowest speeds, with sticking becoming dominant at intermediate speeds, and fragmentation becoming dominant at the higher speeds. Speeds above 1 km s^{-1} can be achieved in such accelerators if more stages are added. This has been done (see Burke et al., 2023, and the discussion above in Sub-Micrometre Particles Section), but so far only for 800 nm particles and impact ionization studies.

As it is, at low speeds, Miller et al. (2022) reported that for ice microparticles impacting molybdenum, 100% rebound at impacts speeds up to 75 m s^{-1}, and the fraction that rebound falls to around zero at around 450 m s^{-1}. Above 75 m s^{-1}, intact (but possibly plastically deformed) particles start sticking to the target, with 80% sticking at speeds of around 200 m s^{-1}, falling to less than 20% at 900 m s^{-1} as fragmentation increasingly occurs instead. From around 125 m s^{-1}, particle fragmentation appears (with some material possibly sticking to the target while the rest rebounds), rising steadily to become the dominant outcome above around 750 m s^{-1}. Using the PIA for ice impacting molybdenum (see Table 1 for relevant coefficients), these speeds correspond to shock pressures as given in Table 2. For ice at higher speeds, Kieffer and Simonds (1980; also see table 3.3 in

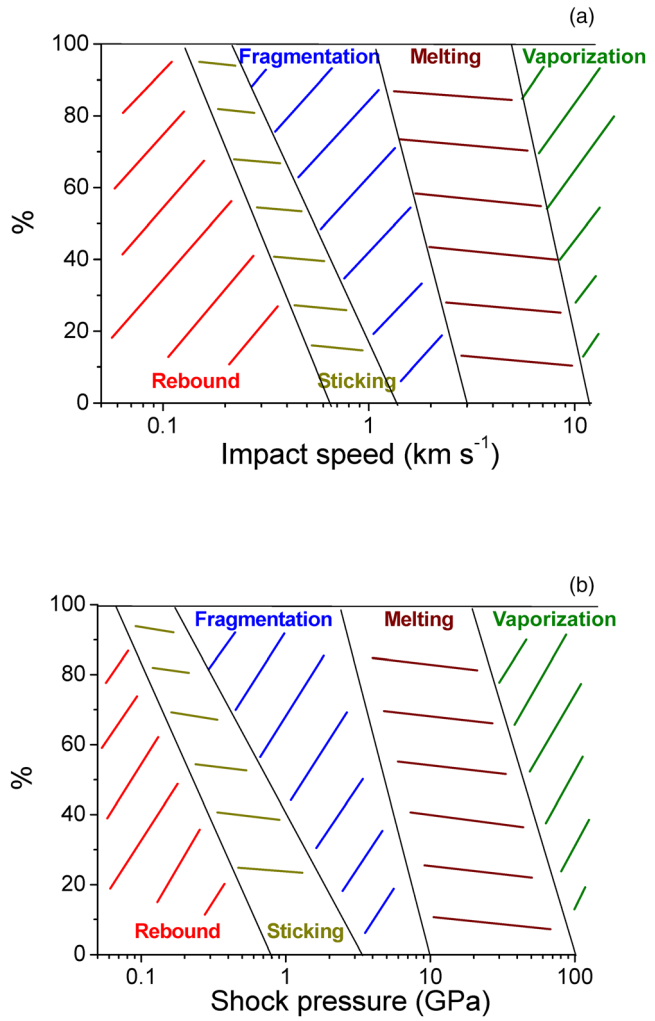

FIGURE 7. Fate under impact of a typical ice/mineral/metal impactor of greater than a few μm in size on a generic solid metal target. The various thresholds are dependent on the composition of both impactor and target. Here the thresholds are given in terms of (a) impact speed at normal incidence and (b) shock pressure (see Table 1).

Melosh, 1989), report that in impacts there is the onset of melting at 3 GPa, with complete melting at 10 GPa, and the onset of vaporization at 26 GPa, with complete vaporization at 100 GPa. For impacts of ice on aluminum, these pressures correspond to onset and complete melting at 1.5 and 3 km s^{-1}, and onset and complete vaporization at 5 and 10.5 km s^{-1}. These thresholds are summarized in Table 2 and shown graphically in Figure 7.

Implications for Plume Sampling Missions

Based on the above, the ability of a space mission to collect materials from a plume depends heavily on the encounter speed, combined with the nature of the impacting material and the target surface. Further complications arise if the energy released in the impact drives chemical synthesis. And, if looking for life itself, the influence of impact shock on the organisms also needs to be considered, with additional critical pressure thresholds for the survival of living material in impacts. Seeds (tobacco, alfalfa, and cress), for example, have been found to fail to germinate after impacts at 1–3 km s^{-1}, involving peak shock pressures of 0.24–2.4 GPa (Jerling et al., 2008). In the lower-speed impacts in Jerling et al. (2008), there was evidence of seeds starting to break apart, but the largest fragments were still similar in size to the original seeds. In the higher-speed shots, the size of the largest fragment after an impact had fallen to typically less than half the size of the original seeds, so although not viable, significant fractions remained intact. Later studies showed that germination rates for cress fell to 25% at 0.3 GPa and to 0% above 0.8 GPa (Leighs et al., 2013), compatible with the earlier work.

The survival of spores and microorganisms in high-speed impact events has also been investigated. Burchell et al. (2000) and Burchell, Shrine, et al. (2001) showed evidence that bacteria (*Rhodococcus erythropolis*) on a projectile could survive after impacts onto rock at 5 km s^{-1}. This was then quantified in a later paper, which showed that at 5 km s^{-1}, spores could impact agar with a survival rate of $\sim 10^{-7}$ (Burchell, Mann, et al., 2001). Via a non-impact method (i.e., explosive-driven shock), Horneck et al. (2001) showed that spores could survive shocks at 38 GPa with a survival rate of $\sim 10^{-4}$. This was then followed by several papers that looked at survival over shock pressure ranges up to 80 GPa (e.g., Burchell et al., 2004; Burchell, 2007; Horneck et al., 2008; Price, Solscheid, et al., 2013). They showed that survival rates for bacteria and spores fall slowly to around 1% up to shock pressures around a few GPa, and then fall more steeply as shock pressure increases. At sub-μm scales, we note that for Cassini CDA at Enceladus, distinctive fragmentation peaks for complex organic materials do not appear in mass spectra below impact speeds of $\sim$5 km s^{-1}, suggesting this is a critical value (Postberg et al., 2018), although the new laboratory data from Burke et al. (2023) suggest that the lower limit may be in the range 3–4 km s^{-1}.

If one wishes to be even more speculative, one can consider how more sophisticated organisms can survive shock impact. Tardigrades are a model organism widely considered for survival in space (e.g., see Lantin et al., 2022 for a discussion). These are hardy organisms, typically around 100 μm in size (but can be larger), which can survive a wide range of environmental stresses (radiation, vacuum, etc.) and can be frozen and successfully defrosted. Although freshwater organisms (whereas the oceans on the IOWs are salt-rich), if they are

taken as a proxy for hardy organisms in general, then in a frozen state we can imagine them ejected in plumes from an IOW. Their survival in impact events has been studied by Traspas and Burchell (2021), who showed that they could be recovered and revived after impacts up to around 0.8–0.9 km s^{-1} with associated shock pressures of 0.9–1.1 GPa. This suggests that an orbiter at Enceladus might well be able to collect such organisms in a viable state, but not orbiters around other IOWs (see Figures 4a and 5).

Alternatively, one can search for macroscopic remnants of life, for example, fossilized structures. If these were carried in frozen droplets in the plumes of an IOW, we can ask if they would be detectable after an impact on a passing spacecraft. This has been considered experimentally for diatoms and foraminifera (see Burchell, McDermott, et al., 2014; Burchell et al., 2017). It was found that, when embedded in ice projectiles (and the foraminifera were also suspended in water during shots), recognizable fossilized diatom and foraminifer structures survived in impacts at speeds up to 6 km s^{-1} (pressures of 20 GPa). This effect was size-dependent, with above about 4 km s^{-1} (10 GPa) the size of the surviving fragments falling below 100 μm. While intact examples over a wide size range were found at lower speeds, any whole, intact examples found in the experiments at the higher speeds and shock pressures were below this size. However, small fragments of larger structures were found at even the highest speeds/pressures. This suggests that recognizable fossilized structures can still be collected if ejected in a plume, but only at small sizes if impact speeds are in the km s^{-1} regime with peak shock pressures of >10 GPa.

Low-Density Collectors

An alternative to collection from plumes via impacts onto normal-density materials is via impacts into layers of thin foils or onto low-density foams or aerogels. All these in effect involve porous targets, with either micro-porosity in the foams and aerogels or macro-porosity between the layers in thin-film targets (see Wozniakiewicz et al., 2021, for a recent review of capture cell technology). Considering the thin foil collectors first, an early example of such a capture cell was the micro-abrasion foil experiment by McDonnell et al. (1984). This used two foil layers, with the first to disrupt the impactor and the second to collect the material. It was flown on the STS-3 Space Shuttle mission in 1984 and obtained evidence of four high-speed impacts, which were analyzed post-flight. The technique is thus valid and can provide impact-disrupted residues on the various layers, which can then be analyzed.

Aerogel, by contrast, is a low-density, micro-porous medium that particles tunnel into on impact, experiencing significantly lower shock pressures than when impacting a normal-density solid (see Burchell et al., 2006, for a discussion of aerogel composition and a review of the use of aerogel as a dust capture medium in space missions). For example, Trigo-Rodríguez et al. (2009) showed that in aerogel with density 20kg m^{-3}, peak shock pressures were of order 0.05 GPa for impacts at 1 km s^{-1}, rising to ~1 GPa at 6 km s^{-1}. Thus, depending on aerogel density and particle composition, projectiles larger than a few μm in size can be captured nearly intact even at impact speeds up to 6 km s^{-1} (e.g., Burchell, Fairey, et al., 2008), and for sub-μm particles, Postberg et al. (2014) have shown that intact capture can occur up to 10 km s^{-1}. Of relevance here is that it has been shown that ice grains can leave tracks in aerogel, similar to mineral, metal, or organic grains (e.g., see Yano et al., 1999 or Burchell et al., 2011).

Probably the best known example of dust capture in aerogel was by the NASA Stardust mission, which collected both cometary (Brownlee et al., 2006; Burchell, Foster, et al., 2008) and interstellar dust samples (Westphal et al., 2014) at 1.5 AU for analysis. A more recent example is as part of the Tanpopo experiments mounted on the outside of the International Space Station, which collected cosmic dust in low Earth orbit (Yamagishi et al., 2021).

When using aerogel in the outer solar system, the ambient temperature might be considered an issue, but it has been shown that the material properties of aerogel are stable over a wide temperature range, that is, 175–600 K (Burchell, Fairey, et al., 2009), so capture should be unaffected. For the Stardust mission, for example, the emphasis was on the mineral content of the dust. But at Enceladus, the organic content will be of great interest, and several issues will arise. The first is that elevated temperatures are produced during capture, which can lead to both surface ablation and processing of the impactor (e.g., Burchell, Foster, et al., 2009). The second issue is that the strength of the particle determines the nature of the capture process in the aerogel. Weak particles, including at least some organic particles, effectively explode during impact, producing very bulbous tracks with no large captured grain; instead, a multitude of small fragments line the cavity wall (Nixon et al., 2012). Finally, the manufacturing process for common aerogels (i.e., SiO_2 aerogel) involves heavy use of organic materials, not all of which are removed during processing, and this can lead to significant organic content of the aerogel itself, which can vary from batch to batch even with the same manufacturing process (see Tsou et al., 2003). However, despite these caveats, it has been shown that microparticles laden with PAHs, for example, can be captured in aerogel at 5.5 km s^{-1}, and mass spectroscopy (with an instrument designed for use

on a space mission) can detect their original organic content (Jones et al., 2015). Also, when analyzed on Earth, the NASA Stardust mission aerogel samples were shown to have collected glycine from material freshly ejected from comet 81P/Wild-2 (Elsila et al., 2009), although detailed isotopic analysis was required to rule out terrestrial contamination.

Orientation of Collector

Even if capture of plume material is in theory feasible at an IOW, the orientation of the collector with respect to the direction of impact is also critical. If the dominant term in the combined spacecraft-plume velocity vector arises from the spacecraft motion, then the passage of the spacecraft through the plume and the orientation of the collector surfaces determine the effective impact direction. However, as already pointed out, for low orbital speeds, such as at Enceladus, the dust grain motion in the plume can be equally significant. This point is important. The impact velocity is a vector quantity, and it is the effective speed at normal incidence that controls peak pressure, for example. Typically, it is taken that an off-normal incidence impact reduces the peak pressure experienced by the impactor by $\sin\theta$, where θ is the angle from the target surface (see Pierazzo & Melosh, 2000 for a review). Thus, an inclination of 45° in the angle of incidence with respect to the collector surface will reduce the peak shock pressure by 30%. Similarly, a shallower impact at 30° (which is usually before any rebound/ricochet effects appear) reduces the peak pressure by 50%.

An off-normal incidence impact also introduces a directional effect in any rebound or ricochet of the impactor. This can be made use of, particularly for low-speed impacts, where a funnel-shaped collector can channel dust onto a smaller specialist capture surface or into a small chamber for collection. This will particularly apply for an Enceladus orbiter.

SAMPLE ANALYSIS

The choice of mission type (flyby, orbiter, lander) and collection method are clearly linked; however, it is also heavily dependent on the information sought and analysis methods required. For example, in high-speed flybys or orbits of the IOW, chemical data can be obtained for micron to sub-micron plume particles that vaporize, permitting the application of impact ionization mass spectroscopy (e.g., the CDA detector on board the Cassini mission, Srama et al., 2004, or the SUDA detector on board the Europa Clipper, Goode et al., 2023; Kempf et al., 2014). However, identification of all materials and species present at all plume particle sizes and all collection speeds requires more careful collection (e.g., via impacts on metal plates or in low-density collectors). This in turn leads to more complex and cumbersome analytical techniques that may ultimately require samples be returned to Earth (due to the size/mass constraints of the current technology or the need for direct human interaction during sample preparation and analysis). However, return to Earth is limited by the constraints of mission planning, that is, the need to escape from the vicinity of Jupiter or Saturn and return to the inner solar system requires a suitable engine and propellant, adding significant mass and cost. Further, as noted earlier, it is also problematic due to the needs of planetary protection (see Present and Future Missions section).

Examples of in situ sample analysis of macroscopic samples collected on spacecraft in space (rather than on the surface of bodies) do exist. For example, the Rosetta mission to comet 67P/Churyumov-Gerasimenko (Glassmeier et al., 2007) orbited the body (collecting samples at low speed) and deployed a lander. On the orbiter, a dust impact detector, Giada, was used to measure the dust flux at the comet, including particle momentum, impact speed ($0.3–35\,m\,s^{-1}$), and particle mass, which ranged from 10^{-9} to 10^{-6} kg (Della Corte et al., 2016; Rotundi et al., 2015). Dust grains were also physically collected by the COSIMA instrument on board Rosetta, which was designed to collect dust at speeds up to $100\,m\,s^{-1}$ (Hornung et al., 2014). The collector surfaces in COSIMA were blocks of microscopic metal grains (<100 nm), which formed a porous metal surface, and which helped capture the incident particles and prevent them rebounding. COSIMA collected several tens of thousands of grains, from sizes of a few 10s of μm to mm scale (Merouane et al., 2016). Analysis was by optical imagery, which provided size distributions and morphology, followed by secondary ion beam mass spectrometry (SIMS). The SIMS data were used to provide m/z spectra for the grains, which gave the broad mineral content of many grains (Hilchenbach et al., 2016) and also the organic content of some grains (Fray et al., 2016), thus showing that, in general, compositional analysis of individual collected dust grains is possible in situ on an orbiting spacecraft. Also on-board was the Micro-Imaging Dust Analysis System (MIDAS), consisting of an atomic force microscope capable of 3-D topographical investigation of collected cometary dust with resolution down to a few nanometers (e.g., Kim et al., 2023).

Unlike Rosetta, where low-impact speeds left intact material on the collector surfaces, at higher-impact speeds, particles may end up lining impact craters as fragments or residues. This presents particular analysis difficulties, as the material to be sampled will now be

inside a crater and not visible at all viewing angles. One technique to present the material for analysis is to use metal foils as targets and then press out the crater from the rear, exposing the residue originally inside the crater back on the original surface plane of the foil (see Wozniakiewicz et al., 2018). This then makes the captured material more readily accessible to the analysis sampling method.

Other complications exist. In the plume of an IOW, much of the solid material will be frozen water. Even in a low-speed impact, to retain the ice grains or their fragments, you will need a cold surface. Further, in many possible mission scenarios, the initial passes of the target IOW may be as flybys during orbits of the parent body, that is, at high speed, say 3–10 km s^{-1}. If a later orbit of the IOW itself then follows, lower speeds will be involved (although for most IOWs they will still be of order 1–2 km s^{-1}). For Enceladus, the contrast in speeds will be even greater, meaning that separate systems may be needed to collect macroscopic impactor material in the flyby and orbiter parts of any missions.

As suggested by several authors (Low Density Collectors Section), aerogel collectors can capture semi-intact grains. However, the extraction of individual grains on Earth from aerogel samples requires detailed, high-resolution microscopy combined with delicate extraction techniques to cut the particle and its track out of the parent aerogel. This is not currently possible on a robotic spacecraft. Instead, after imaging to locate the larger particles, aerogel samples will likely need to be crushed for a bulk averaged analysis. That this can be successfully done was shown by Jones et al. (2015).

Whatever the collection system, one remaining issue is how often to trigger the particle extraction for analysis. Should it be on each pass through the plume? Or after many passes to allow the accumulation of material? In the former case, if the mission is in orbit around the IOW, the orbital period becomes crucial. In the latter case, preserving any icy material for extended periods is key.

When designing a mission to the IOWs, the mission type and sampling/analysis methods will thus together determine the range of questions that can be addressed. Furthermore, the issue of sample preparation for analysis is crucial.

CONCLUSIONS

This paper has focused on the bodies where there is sufficient evidence to support internal oceans. As well as interest in the physical characterization of these bodies, they are also of great astrobiological interest due to the presence of liquid water. It should be no surprise, therefore, that a wide range of space missions to these bodies have been proposed or are underway.

Whatever target IOW and mission architecture is involved, if future missions do indeed aim to collect material from the plumes (or from impact ejecta) at an IOW, the issues described here relating to collection speed, peak shock pressures and the consequent impact processing of the collected material, will be highly relevant.

Acknowledgments—We thank STFC for funding (grant numbers ST/N000854/1 and ST/S000348/1). We thank the referees for their supportive comments and suggestions on the manuscript.

Conflict of Interest Statement—There are no competing interests.

Data Availability Statement—Data sharing not applicable to this article as no datasets were generated or analysed during the current study.

Editorial Handling—Dr. Daniel Patrick Glavin

REFERENCES

Ahrens, T. J., and Johnson, M. L. 1995. Shock Wave Data for Rocks. In *AGU Reference Shelf 3: Rock Physics and Phase Relations, A Handbook of Physical Constants*, edited by T. J. Ahrens, 35–44. Washington, DC: American Geophysical Union.

Anders, C., Bringers, E. M., and Urbassek, H. M. 2020. Ejection of Glycine Molecules Adsorbed on a Water Ice Surface by Swift-Heavy Ion Irradiation. *The Astrophysical Journal* 891: 21. https://doi.org/10.3847/1538-4357/ab6efe.

Bar-Nun, A., Bar-Nun, N., Bauer, S., and Sagan, C. 1970. Shock Synthesis of Amino Acids in Simulated Primitive Environments. *Science* 168: 470–72.

Béghin, C., Randriamboarison, O., Hamelin, M., Karkoschka, E., Sotin, C., Whitten, R. C., Berthelier, J. J., Grard, R., and Simões, F. 2012. Analytic Theory of Titan's Schumann Resonance: Constraints on Ionospheric Conductivity and Buried Water Ocean. *Icarus* 218: 1028–42.

Bierson, C. J., Nimmo, F., and Stern, S. A. 2020. Evidence for a Hot Start and Early Ocean Formation on Pluto. *Nature Geoscience* 13: 468–472.

Blank, J. G., Miller, G. H., Ahrens, M. J., and Winans, R. E. 2001. Experimental Shock Chemistry of Aqueous Amino Acid Solutions and the Cometary Delivery of Prebiotic Compounds. *Origins of Life and Evolution of the Biosphere* 31: 15–51.

Bowden, S. A., Parnell, J., and Burchell, M. J. 2009. Survival of Organic Compounds in Ejecta from Hypervelocity Impacts on Ice. *International Journal of Astrobiology* 8: 19–25.

Brownlee, D. E., Tsou, P., Aléon, J., Alexander, C. M. O'D., Araki, T., Bajt, S., Baratta, G. A., et al. 2006. Comet Wild-2 under a Microscope. *Science* 314: 1711–16.

Burchell, M., and Harriss, K. 2020. Organic Molecules: Is it Possible to Distinguish Aromatics from Aliphatics Collected by Space Missions in High Speed Impacts? *Science* 2: 56. https://doi.org/10.3390/sci2030056.

Burchell, M. J. 2007. Survival of Microbial Life Under Shock Compression: Implications for Panspermia. Proceedings of SPIE Symposium 6694, Instruments, Methods, and Missions for Astrobiology X, Identifier 669416, 10 p https://doi.org/10.1117/12.732369.

Burchell, M. J., and Armes, S. P. 2011. Impact Ionization Spectra from Aliphatic PMMA Microparticles. *Rapid Communications in Mass Spectroscopy* 25: 543–550.

Burchell, M. J., Bowden, S. A., Cole, M., Price, M. C., and Parnell, J. 2014. Survival of Organic Materials in Hypervelocity Impacts of Ice on Sand, Ice and Water in the Laboratory. *Astrobiology* 14: 473–485.

Burchell, M. J., Cole, M. C., Price, M. C., and Kearsley, A. T. 2011. Ice Impacts on Aerogel and Stardust Al Foil. *Meteoritics & Planetary Science Supplement* 46: A34.

Burchell, M. J., Cole, M. J., McDonnell, J. A. M., and Zarnecki, J. C. 1999. Hypervelocity Impact Studies Using the 2 MV Van de Graaff Dust Accelerator and Two Stage Light Gas Gun of the University of Kent at Canterbury. *Measurement Science and Technology* 10: 41–50.

Burchell, M. J., Cole, M. J., and Ratcliff, P. R. 1996. Light Flash and Ionization from Hypervelocity Impacts on Ice. *Icarus* 122: 359–365.

Burchell, M. J., Fairey, S. A. J., Foster, N. J., and Cole, M. J. 2009. Hypervelocity Capture of Particles in Aerogel: Dependence on Aerogel Properties. *Planetary and Space Science* 57: 58–70.

Burchell, M. J., Fairey, S. A. J., Wozniakiewicz, P., Brownlee, D. E., Hörz, F., Kearsley, A. T., See, T. H., Westphal, A., Green, S. F., and Trigo-Rodríguez, J. M. 2008. Characteristics of Cometary Dust Tracks in Stardust Aerogel and Laboratory Calibrations. *Meteoritics & Planetary Science* 43: 23–40.

Burchell, M. J., Foster, N. J., Kearsley, A. T., and Creighton, J. A. 2008. Identification of Mineral Impactors in Hypervelocity Impact Craters in Aluminium by Raman Spectroscopy of Residues. *Meteoritics & Planetary Science* 43: 135–142.

Burchell, M. J., Foster, N. J., Ormond-Prout, J., Dupin, D., and Armes, S. P. 2009. Extent of Thermal Ablation Suffered by Model Organic Microparticles during Aerogel Capture at Hypervelocities. *Meteoritics & Planetary Science* 44: 1407–20.

Burchell, M. J., Graham, G., and Kearsley, A. 2006. Cosmic Dust Collection in Aerogel. *Annual Reviews of Earth and Planetary Science* 34: 385–418.

Burchell, M. J., Harriss, K. H., Price, M. C., and Yolland, L. 2017. Survival of Fossilised Diatoms and Forams in Hypervelocity Impacts with Peak Shock Pressures in the 1–19 GPa Range. *Icarus* 290: 81–88.

Burchell, M. J., and Kearsley, A. T. 2009. Short Period Jupiter Family Comets after Stardust. *Planetary and Space Science* 57: 1146–61.

Burchell, M. J., Mann, J., Bunch, A. W., and Brandão, P. F. B. 2001. Survivability of Bacteria in Hypervelocity Impact. *Icarus* 154: 545–47.

Burchell, M. J., Mann, J. R., and Bunch, A. W. 2004. Survival of Bacteria and Spores under Extreme Pressures. *Monthly Notices of the Royal Astronomical Society* 352: 1273–78.

Burchell, M. J., McDermott, K. H., and Price, M. C. 2014. Survival of Fossils under Extreme Shocks Induced by Hypervelocity Impacts. *Philosophical Transactions of the Royal Society A* 372: 20130190.

Burchell, M. J., Shrine, N. R. G., Bunch, A., and Zarnecki, Z. 2000. Experimental Tests of the Impact Related Aspects of Panspermia. In *Impacts on the Early Earth*, edited by I. Gilmour, and C. Koeberl, 1–26. Berlin, Heidelberg, New York: Springer-Verlag. ISBN 3-540-67092-0.

Burchell, M. J., Shrine, N. R. G., Mann, J., Bunch, A. W., Brandão, P., Zarnecki, J., and Galloway, J. A. 2001. Laboratory Investigations of the Survivability of Bacteria in Hypervelocity Impacts. *Advances in Space Research* 28: 707–712.

Burke, S. E., Auvil, Z. A., Hanold, K. A., and Continetti, R. E. 2023. Detection of Intact Amino Acids with a Hypervelocity Ice Grain Impact Mass Spectrometer. *Proceedings of the National Academy of Sciences of the United States of America* 120: e2313447120. https://doi.org/10.1073/pnas.2313447120.

Čadek, O., Tobie, G., Van Hoolst, T., Masse, M., Choblet, G., Lefevre, A., Mitri, G., et al. 2016. Enceladus's Internal Ocean and Ice Shell Constrained from Cassini Gravity, Shape, and Libration Data. *Geophysical Research Letters* 43: 5653–60.

Carr, M. H., Belton, M. J., Chapman, C. R., Davies, M. E., Geissler, P., Greenberg, R., and Veverka, J. 1998. Evidence for a Subsurface Ocean on Europa. *Nature* 391: 363–65.

Castillo-Rogez, J. C., Neveu, M., Scully, J. E. C., House, C. H., Quick, L. C., Bouquet, A., Miller, K., et al. 2020. Ceres: Astrobiological Target and Possible Ocean World. *Astrobiology* 20: 269–291. https://doi.org/10.1089/ast.2018.1999.

Chan, D. H., Millet, A., Fisher, C. R., Price, M. C., Burchell, M. J., and Armes, S. P. 2021. Synthesis and Characterization of Polypyrrole-Coated Anthracene Microparticles: A New Synthetic Mimic for Polyaromatic Hydrocarbon-Based Cosmic Dust. *ACS Applied Materials & Interfaces* 13: 3175–85. https://doi.org/10.1021/acsami.0c19758.

Chan, D. H. H., Wills, J. L., Tandy, J. D., Burchell, M. J., Wozniakiewicz, P. J., Alesbrook, L. S., and Armes, S. P. 2023. Synthesis of Autofluorescent Phenanthrene Microparticles Via Emulsification: A Useful Synthetic Mimic for Polycyclic Aromatic Hydrocarbon-Based Cosmic Dust. *ACS Applied Materials & Interfaces* 15: 54039–49.

COSPAR. 2021. COSPAR Policy on Planetary Protection https://cosparhq.cnes.fr/assets/uploads/2021/07/PPPolicy_2021_3-June.pdf.

Dalmann, B. K., Grün, E., Kissel, J., and Dietzel, H. 1977. The Ion Composition of the Plasma Produced by Impacts of Fast Dust Particles. *Planetary and Space Science* 25: 135–147.

Degruyter, W., and Manga, M. 2011. Cryoclastic Origin of Particles on the Surface of Enceladus. *Geophysical Research Letters* 38: L16201.

Della Corte, V., Rotundi, A., Fulle, M., Ivanovski, S., Green, S. F., Rietmeijer, F. J. M., Colangeli, L., et al. 2016. 67P/C-G Inner Coma Dust Properties from 2.2 au Inbound to 2.0 au Outbound to the Sun. *Monthly Notices of the Royal Astronomical Society* 462: S210–S219. https://doi.org/10.1093/mnras/stw2529.

Drapatz, S., and Michel, K.-W. 1974. Theory of Shock-Wave Ionization upon High-Velocity Impact of Micrometeorites.

Zeitschrift Naturforschung A 29: 870–79. https://doi.org/10.1515/zna-1974-0606.

Elsila, J. E., Glavin, D. P., and Dworkin, J. P. 2009. Cometary Glycine Detected in Samples Returned by Stardust. *Meteoritics & Planetary Science* 44: 1313–30.

Enceladus Orbilander. 2021. Planetary Mission Concept Study for the 2023–2032 Decadal Survey: A Flagship Mission Concept for Astrobiology https://ntrs.nasa.gov/api/citations/20205008712/downloads/enceladusorbilander_2020pmcs.pdf.

Fantino, E., Salazar, F., and Alessi, E. M. 2020. Design and Performance of Low-Energy Orbits for the Exploration of Enceladus. *Communications in Nonlinear Science and Numerical Simulation* 90: 105393. https://doi.org/10.1016/j.cnsns.2020.105393.

Fiege, K., Trieloff, M., Hillier, J. K., Guglielmino, M., Postberg, F., Srama, R., Kempf, S., and Blum, J. 2014. Calibration of Relative Sensitivity Factors for Impact Ionization Detectors with High-Velocity Silicate Microparticles. *Icarus* 241: 336–345. https://doi.org/10.1016/j.icarus.2014.07.015.

Fielding, L. A., Hillier, J. K., Burchell, M. J., and Armes, S. P. 2015. Space Science Applications for Conducting Polymer Particles: Synthetic Mimics for Cosmic Dust and Micrometeorites. *Chemical Communications* 51: 16886–99.

Fisher, C. R., Price, M. C., and Burchell, M. J. 2021. Salt Grains in Hypervelocity Impacts in the Laboratory. *Meteoritics & Planetary Science* 56: 1652–68. https://doi.org/10.1111/maps.13729.

Fray, N., Bardyn, A., Cottin, H., Altwegg, K., Baklouti, D., Briois, C., Colangeli, L., et al. 2016. High-Molecular-Weight Organic Matter in the Particles of Comet 67P/Churyumov–Gerasimenko. *Nature* 538: 72–74. https://doi.org/10.1038/nature19320.

Gaeman, J., Hier-Majumder, S., and Roberts, J. H. 2012. Sustainability of a Subsurface Ocean within Triton's Interior. *Icarus* 220: 339–347.

Glassmeier, K. H., Boehnhardt, H., Koschny, D., Kührt, E., and Richter, I. 2007. The Rosetta Mission: Flying Towards the Origin of the Solar System. *Space Science Reviews* 128: 1–21. https://doi.org/10.1007/s11214-006-9140-8.

Goldstein, D. B., Hedman, M., Manga, M., Perry, M., Spitale, J., and Teolis, B. 2018. Enceladus Plume Dynamics. In *Enceladus and the Icy Moons of Saturn*, edited by P. M. Schenk, R. N. Clark, C. J. A. Howett, J. A. Verbiscer, and J. H. Waite, 175–194. Tucson, AZ: University of Arizona. https://doi.org/10.2458/azu_uapress_9780816537075-ch005.

Goldsworthy, B. J., Burchell, M. J., Cole, M. J., Armes, S. P., Khan, M. A., Lascelles, S. F., Green, S. F., McDonnell, J. A. M., Srama, R., and Bigger, S. W. 2003. Time of Flight Mass Spectrometry of Ions in Plasmas Produced by Hypervelocity Impacts of Organic and Mineralogical Microparticles on a Cosmic Dust Analyser. *Astronomy & Astrophysics* 409: 1151–67.

Goldsworthy, B. J., Burchell, M. J., Cole, M. J., Green, S. F., Leese, M. R., McBride, N., McDonnell, J. A. M., et al. 2002. Laboratory Calibration of the Cassini Cosmic Dust Analyser (CDA) Using New Low Density Projectiles. *Advances in Space Research* 29: 1139–44.

Goode, W., Kempf, S., and Schmidt, J. 2023. Mapping the Surface Composition of Europa with SUDA. *Planetary and Space Science* 227: 2023. https://doi.org/10.1016/j.pss.2023.105633.

Grasset, O., Dougherty, M. K., Coustenis, A., Bunce, E. J., Erd, C., Titov, D., Blanc, M., et al. 2013. JUpiter ICy Moons Explorer (JUICE): An ESA Mission to Orbit Ganymede and to Characterise the Jupiter System. *Planetary and Space Science* 78: 1–21.

Guzman, M., Lorenz, R., Hurley, D., Farrell, W., Spencer, J., Hansen, C., Hurford, T., Ibea, J., Carlson, P., and McKay, C. P. 2019. Collecting Amino Acids in the Enceladus Plume. *International Journal of Astrobiology* 18: 47–59.

Hall, S. 2015. Soaked in Space. *Scientific American* 314: 14–15. https://doi.org/10.1038/scientificamerican0116-14.

Hand, K. P., Sotin, C., Hayes, A., and Coustenis, A. 2020. On the Habitability and Future Exploration of Ocean Worlds. *Space Science Reviews* 216: 24.

Hand, K. P., et al. 2017. Europa Lander Study 2016 Report: Europa Lander Mission, JPL D-97667 (NASA, Washington, DC, USA). https:/europa.nasa.gov/resources/58/europa-lander-study-2016-report/.

Hansen, C. J., Esposito, L., Stewart, A. I. F., Colwell, J., Hendrix, A., Pryor, W., Shemansky, D., and West, R. 2006. Enceladus' Water Vapor Plume. *Nature* 311: 1422–25.

Hansen, C. J., Esposito, L. W., Colwell, J. E., Hendrix, A. R., Portyankina, G., Stewart, A. I. F., and West, R. A. 2020. The Composition and Structure of Enceladus' Plume from the Complete Set of Cassini UVIS Occultation Observations. *Icarus* 344: 113461. https://doi.org/10.1016/j.icarus.2019.113461.

Hemingway, D., Iess, L., Tajeddine, R., and Tobie, G. 2018. The Interior of Enceladus. In *Enceladus and the Icy Moons of Saturn*, edited by P. M. Schenk, R. N. Clark, C. J. A. Howett, J. A. Verbiscer, and J. H. Waite, 57–77. Tucson, AZ: University of Arizona. https://doi.org/10.2458/azu_uapress_9780816537075-ch004.

Hemingway, D., Nimmo, F., Zebker, H., and Iess, L. 2013. A Rigid and Weathered Ice Shell on Titan. *Nature* 500: 550–52.

Hemingway, D. J., and Mittal, T. 2019. Enceladus's Ice Shell Structure as a Window on Internal Heat Production. *Icarus* 332: 111–131. https://doi.org/10.1016/j.icarus.2019.03.011.

Hendrix, A. R., Hurford, T. A., Barge, L. M., Bland, M. T., Bowman, J. S., Brinckerhoff, W., Buratti, B. J., et al. 2019. The NASA Roadmap to Ocean Worlds. *Astrobiology* 19: 1–27.

Hilchenbach, M., Kissel, J., Langevin, Y., Briois, C., Hoerner, H., Koch, A., Schulz, R., et al. 2016. Comet 67P/Churyumov–Gerasimenko: Close-Up on Dust Particle Fragments. *The Astrophysical Journal* 816: L32.

Hillier, J. K., Green, S. F., McBride, N., Schwanethal, J. P., Postberg, F., Srama, R., Kempf, S., Moragas-Klostermeyer, G., McDonnell, J. A. M., and Grün, E. 2007. The Composition of Saturn's E Ring. *Monthly Notices of the Royal Astronomical Society* 377: 1588–96. https://doi.org/10.1111/j.1365-2966.2007.11710.x.

Hillier, J. K., Postberg, F., Sestak, S., Srama, R., Kempf, S., Trieloff, M., Sternovsky, Z., and Green, S. F. 2012. Impact Ionization Mass Spectra of Anorthite Cosmic Dust Analogue Particles. *Journal of Geophysical Research* 117: E09002. https://doi.org/10.1029/2012JE004077.

Hillier, J. K., Sternovsky, Z., Armes, S. P., Fielding, L. A., Postberg, F., Bugiel, S., Drake, K., Srama, R., Kearsley, A. T., and Trieloff, M. 2014. Impact Ionisation Mass Spectrometry of Polypyrrole-Coated Pyrrhotite

Microparticles. *Planetary and Space Science* 97: 9–22. https://doi.org/10.1016/j.pss.2014.04.008.
Hofgartner, J. D., Birch, S. P. D., Castillo, J., Grundy, W. M., Hansen, C. J., Hayes, A. G., Howett, C. J. A., et al. 2022. Hypotheses for Triton's Plumes: New Analyses and Future Remote Sensing Tests. *Icarus* 375: 114835.
Horneck, G., Stöffler, D., Eschweiler, U., and Hornemann, U. 2001. Bacterial Spores Survive Simulated Meteorite Impact. *Icarus* 149: 285–290.
Horneck, G., Stöffler, D., Ott, S., Hornemann, U., Eschweiler, U., Cockell, C. S., Moeller, R., et al. 2008. Microbial Rock Inhabitants Survive Hypervelocity Impacts on Mars-Like Host Planets: First Phase of Lithopanspermia Experimentally Tested. *Astrobiology* 8: 17–44.
Hornung, K., Kissel, J., Fischer, H., Mellado, E. M., Kulikov, O., Hilchenbach, M., Krüger, H., et al. 2014. Collecting Cometary Dust Particles on Metal Blacks with the COSIMA Instrument Onboard ROSETTA. *Planetary and Space Science* 103: 309–317.
Hsu, H.-W., Postberg, F., Sekine, Y., Shibuya, T., Kempf, S., Horányi, M., Juhász, A., et al. 2015. Ongoing Hydrothermal Activities within Enceladus. *Nature* 519: 207–210. https://doi.org/10.1038/nature14262.
Hussmann, H., Sohl, F., and Spohn, T. 2006. Subsurface Oceans and Deep Interiors of Medium-Sized Outer Planet Satellites and Large Trans-Neptunian Objects. *Icarus* 185: 258–273.
Iess, L., Stevenson, D. J., Parisi, M., Hemingway, D., Jacobson, R. A., Lunine, J. I., Nimmo, F., et al. 2014. The Gravity Field and Interior Structure of Enceladus. *Science* 344: 78–80. https://doi.org/10.1126/science.1250551.
Jaramillo-Botero, A., Cable, M. L., Hofmann, A. E., Malaska, M., Hodyss, R., and Lunine, J. 2021. Understanding Hypervelocity Sampling of Biosignatures in Space Missions. *Astrobiology* 21: 421–442. https://doi.org/10.1089/ast.2020.2301.
Jerling, A., Burchell, M. J., and Tepfer, D. 2008. Survival of Seeds in Hypervelocity Impacts. *International Journal of Astrobiology* 7: 217–222.
Jia, X., Kivelson, M. G., Khurana, K. K., and Kurth, W. S. 2018. Evidence of a Plume on Europa from Galileo Magnetic and Plasma Wave Signatures. *Nature Astronomy* 2: 459–464. https://doi.org/10.1038/s41550-018-0450-z.
Johnson, R. E., and Sundqvist, B. U. R. 2018. Sputtering and Detection of Large Organic Molecules from Europa. *Icarus* 309: 338–344. https://doi.org/10.1016/j.icarus.2018.01.027.
Jones, S., Anderson, M. S., Davies, A. G., Kirby, J. P., Burchell, M. J., and Cole, M. J. 2015. Aerogel Dust Collection for In Situ Mass Spectroscopic Analysis. *Icarus* 247: 71–76.
Jordan, J. L., Casem, D., and Zellner, M. 2016. Shock Response of Polymethylmeth-Acrylate. *Journal of Dynamic Behavior of Materials* 2: 372–78.
Kearsley, A. T., Graham, G. A., Burchell, M. J., Cole, M. J., Dai, Z., Teslich, N., Chater, R. J., Wozniakiewicz, P. J., Spratt, J., and Jones, G. 2007. Analytical Scanning and Transmission Electron Microscopy of Laboratory Impacts on Stardust Aluminium Foils: Interpreting Impact Crater Morphology and the Composition of Impact Residues. *Meteoritics & Planetary Science* 42: 191–210. https://doi.org/10.1111/j.1945-5100.2007.tb00227.x.
Kempf, S., Altobelli, N., Briois, C., Grün, E., Horanyi, M., Postberg, F., Schmidt, J., et al. 2014. SUDA: A Dust Mass Spectrometer for Compositional Surface Mapping for a Mission to Europa. European Planetary Science Congress 9, EPSC2014-229.
Khawaja, N., Postberg, F., Hillier, J., Klenner, F., Kempf, S., Nölle, L., Reviol, L. R., Zou, Z., and Srama, R. 2019. Low Mass Nitrogen-, Oxygen-Bearing, and Aromatic Compounds in Enceladean Ice Grains. *Monthly Notices of the Royal Astronomical Society* 489: 5231–43.
Khurana, K. K., Kivelson, M. G., Stevenson, D. J., Schubert, G., Russell, C. T., Walker, R. J., and Polanskey, C. 1998. Induced Magnetic Fields as Evidence for Subsurface Oceans in Europa and Callisto. *Nature* 395: 777–780.
Kieffer, S. W., and Simonds, C. H. 1980. The Role of Volatiles and Lithology in the Impact Cratering Process. *Reviews of Geophysics and Space Physics* 18: 143–181.
Kim, M., Mannel, T., Boakes, P. D., Bentley, M. S., Longobardo, A., Jeszenszky, H., Moissl, R., and the MIDAS team. 2023. Cometary Dust Collected by MIDAS on Board Rosetta – I Dust Particle Catalog and Statistics. *Astronomy & Astrophysics* 673: A129. https://doi.org/10.1051/0004-6361/202245262.
Kissel, J., and Krueger, F. R. 1987. Ion Formation by Impact of Fast Dust Particles and Comparison with Related Techniques. *Applied Physics A: Materials Science & Processing* 42: 69–85.
Kivelson, G., Khurana, K. K., and Volwerk, M. 2002. The Permanent and Inductive Magnetic Moments of Ganymede. *Icarus* 157: 507–522.
Kivelson, M. G., Khurana, K. K., Russell, C. T., Volwerk, M., Walker, R. J., and Zimmer, C. 2000. Galileo Magnetometer Measurements: A Stronger Case for a Subsurface Ocean at Europa. *Science* 289: 1340–43. https://doi.org/10.1126/science.289.5483.1340.
Klenner, F., Postberg, F., Hillier, J., Khawaja, N., Cable, M. L., Abel, B., Kempf, S., et al. 2020. Discriminating Abiotic and Biotic Fingerprints of Amino Acids and Fatty Acids in Ice Grains Relevant to Ocean Worlds. *Astrobiology* 20: 1168–84.
Klenner, F., Postberg, F., Hillier, J., Khawaja, N., Reviol, R., Srama, R., Abel, B., Stolz, F., and Kempf, S. 2019. Analogue Spectra for Impact Ionization Mass Spectra of Water Ice Grains Obtained at Different Impact Speeds in Space. *Rapid Communications in Mass Spectrometry* 33: 1751–60.
Kotlarz, J., Zielenkiewicz, U., Zalewska, N. E., and Kubiak, K. A. 2020. Microbial Component Detection in Enceladus Snowing Phenomenon. *Astrophysical Bulletin* 75: 166–175.
Lantin, S., Mendell, S., Akkad, G., Cohen, A. N., Apicella, X., McCoy, E., Eliana Beltran-Pardo, E., et al. 2022. Interstellar Space Biology Via Project Starlight. *Acta Astronautica* 190: 261–272.
Leighs, J. A., Hazell, P. J., and Appleby-Thomas, G. J. 2013. The Effect of Shock Loading on the Survival of Plant Seeds. *Icarus* 220: 23–28.
Lesage, E., Massol, H., Howell, S. M., and Schmidt, F. 2022. Simulation of Freezing Cryomagma Reservoirs in Viscoelastic Ice Shells. *The Planetary Science Journal* 3: 170 (15 pp).
Lorenz, R., and Burk, T. A. 2018. Enceladus Plume Density from Cassini Spacecraft Attitude Control Data. *Icarus* 300: 200–202.
Lorenz, R. D. 2016. Europa Ocean Sampling by Plume Flythrough: Astrobiological Expectations. *Icarus* 267: 217–19.
Lorenz, R. D., Stiles, B., Kirk, R. L., Allison, M. D., del Marmo, P., Iess, L., Lunine, J. I., Ostro, S. J., and

Hensley, S. 2008. Titan's Rotation Reveals an Internal Ocean and Changing Zonal Winds. *Science* 319: 1649–51.

Lowell, R. P., and DuBose, M. 2005. Hydrothermal Systems on Europa. *Geophysical Research Letters* 32: L05202. https://doi.org/10.1029/2005GL022375.

MacKenzie, S. M., Neveu, M., Davila, A. F., Lunine, J. I., Cable, M. J., Phillips-Lander, C. M., Eigenbrode, J. L., et al. 2022. Science Objectives for Flagship-Class Mission Concepts for the Search for Evidence of Life at Enceladus. *Astrobiology* 22: 685–712.

MacKenzie, S. M., Neveu, M., Davila, A. F., Lunine, J. I., Craft, K. L., Cable, M. L., Phillips-Lander, C. M., et al. 2021. The Enceladus Orbilander Mission Concept: Balancing Return and Resources in the Search for Life. *The Planetary Science Journal* 2: 77 (18 pp). https://doi.org/10.3847/PSJ/abe4da.

Martins, Z., Price, M. C., Goldman, N., Sephton, M. A., and Burchell, M. J. 2013. Shock Synthesis of Amino Acids from Impacting Cometary and Icy Planet Surface Analogues. *Nature Geoscience* 6: 1045–49.

Massarweh, L., and Cappuccio, P. 2020. On the Restricted 3-Body Problem for the Saturn-Enceladus System: Mission Geometry & Orbit Design for Plume Sampling Missions. *AIAA SciTech Forum* 0467. https://doi.org/10.2514/6.2020-0467.

McDonnell, J. A. M., Carey, W. C., and Dixon, D. G. 1984. Cosmic Dust Collection by the Capture Cell Technique on the Space Shuttle. *Nature* 309: 237–240.

Mellado, E. M., Hornung, K., Srama, R., Kissel, J., Armes, S. P., and Fujii, S. 2011. Mass Spectrometry of Impact Fragmented Polymers: The Role of Target Properties. *International Journal of Impact Engineering* 38: 486–494. https://doi.org/10.1016/j.ijimpeng.2010.10.020.

Melosh, H. J. 1989. *Impact Cratering: A Geologic Process*. New York, NY: Oxford University Press. 245.

Melosh, H. J. 2013. The Contact and Compression Stage of Impact Cratering. In *Impact Cratering: Processes and Products*, edited by G. R. Osinski, and E. Pierazzo. West Sussex, UK: Wiley-Blackwell, Chapter 3, pp. 32–42.

Merouane, S., Zaprudin, B., Stenzel, O., Langevin, Y., Altobelli, N., Della Corte, V., Fischer, H., et al. 2016. Dust Particle Flux and Size Distribution in the Coma of 67P/Churyumov-Gerasimenko Measured In Situ by the COSIMA Instrument on Board Rosetta. *Astronomy and Astrophysics* 596: A87. https://doi.org/10.1051/0004-6361/201527958.

Miller, M. E. C., Burke, S. E., and Continetti, R. E. 2022. Production and Impact Characterization of Enceladus Ice Grain Analogues. *ACS Earth and Space Chemistry* 6: 1813–32. https://doi.org/10.1021/acsearthspacechem.2c00087.

Mitri, G., Postberg, F., Soderblom, J. M., Wurz, P., Tortora, P., Abel, B., Barnes, J. W., et al. 2018. Explorer of Enceladus and Titan (E^2T): Investigating Ocean Worlds' Evolution and Habitability in the Solar System. *Planetary and Space Science* 155: 73–90. https://doi.org/10.1016/j.pss.2017.11.001.

Mousis, O., Bouquet, A., Langevin, Y., André, N., Boithias, H., Durry, G., Faye, F., et al. 2022. Moonraker: Enceladus Multiple Flyby Mission. *Planetary Science Journal* 3: 268 (12 pp). https://doi.org/10.3847/PSJ/ac9c03.

National Academies of Sciences, Engineering, and Medicine. 2022. *Origins, Worlds, and Life: A Decadal Strategy for Planetary Science and Astrobiology 2023–2032*. Washington, DC: The National Academies Press. https://doi.org/10.17226/26522.

New, J. S., Bahar, K., Spathis, V., Price, M. C., Mathies, R. A., and Butterworth, A. L. 2021. Quantitative Evaluation of the Feasibility of Sampling the Ice Plumes at Enceladus for Biomarkers of Extraterrestrial Life. *Proceedings of the National Academy of Sciences of the United States of America* 118: e2106197118. https://doi.org/10.1073/pnas.2106197118.

New, J. S., Mathies, R. A., Price, M. C., Cole, M. J., Golozar, M., Spathis, V., Burchell, M. J., and Butterworth, A. L. 2020. Characterizing Organic Particle Impacts on Inert Metal Surfaces: Foundations for Capturing Organic Molecules during Hypervelocity Transits of Enceladus Plumes. *Meteoritics & Planetary Science* 55: 465–479. https://doi.org/10.1111/maps.13448.

Nimmo, F., Hamilton, D. P., McKinnon, W. P., Schenk, P. M., Binzel, R. P., Bierson, C. J., Beyer, R. A., et al. 2016. Reorientation of Sputnik Planitia Implies a Subsurface Ocean on Pluto. *Nature* 540: 94–96.

Nimmo, F., and Pappalardo, R. T. 2016. Ocean Worlds in the Outer Solar System. *Journal of Geophysical Research, Planets* 121: 1378–99. https://doi.org/10.1002/2016JE005081.

Nimmo, F., Spencer, J. R., Pappalardo, R. T., and Mullen, M. E. 2007. Shear Heating as the Origin of the Plumes and Heat Flux on Enceladus. *Nature* 447: 289–291.

Nixon, A., Burchell, M. J., Price, M. C., Kearsley, A. T., and Jones, S. 2012. Aerogel Tracks Made by Impacts of Glycine: Implications for Formation of Bulbous Tracks in Aerogel and the Stardust Mission. *Meteoritics & Planetary Science* 47: 623–633.

Nna-Mvondo, D., Khare, B., Ishihara, T., and McKay, C. P. 2008. Experimental Impact Shock Chemistry on Planetary Icy Satellites. *Icarus* 194: 822–835.

Pappalardo, R. T., Belton, M. J. S., Breneman, H. H., Carr, M. H., Chapman, C. R., Collins, G. C., and Williams, K. K. 1999. Does Europa have a Subsurface Ocean? Evaluation of the Geological Evidence. *Journal of Geophysical Research: Planets* 104(E10): 24015–55.

Peterson, E., Horz, F., and Chang, S. 1997. Modification of Amino Acids at Shock Pressures of 3.5 to 32 GPa. *Geochimica et Cosmochimica Acta* 61: 3937–50.

Pierazzo, E., and Melosh, H. J. 2000. Understanding Oblique Impacts from Experiments, Observations, and Modeling. *Annual Review of Earth and Planetary Sciences* 28: 141–167.

Porco, C. C., Dones, L., and Mitchell, C. 2017. Could it be Snowing Microbes on Enceladus? Assessing Conditions in its Plume and Implications for Future Missions. *Astrobiology* 17: 876–901.

Porco, C. C., Helfenstein, P., Thomas, P. C., Ingersoll, A. P., Wisdom, J., West, R., Neukum, G., et al. 2006. Cassini Observes the Active South Pole of Enceladus. *Nature* 311: 1393–1401.

Postberg, F., Hillier, J. K., Armes, S. P., Bugiel, S., Butterworth, A., Dupin, D., Fielding, L. A., et al. 2014. Stardust Interstellar Preliminary Examination IX: High-Speed Interstellar Dust Analog Capture in Stardust Flight-Spare Aerogel. *Meteoritics & Planetary Science* 49: 1666–79. https://doi.org/10.1111/maps.12173.

Postberg, F., Kempf, S., Hillier, J. K., Srama, R., Green, S. F., McBride, N., and Grün, E. 2008. The E-Ring in the Vicinity of Enceladus: II. Probing the Moon's Interior—The Composition of E-Ring Particles. *Icarus* 193: 438–454.

Postberg, F., Kempf, S., Schmidt, J., Brilliantov, N., Beinsen, A., Abel, B., Buck, U., and Srama, R. 2009. Sodium Salts in E Ring Ice Grains from an Ocean below the Surface of Enceladus. *Nature* 459: 1098–2001.

Postberg, F., Khawaja, N., Abel, B., Choblet, G., Glein, C. R., Gudipati, M. S., Henderson, B. L., et al. 2018. Macromolecular Organic Compounds from the Depths of Enceladus. *Nature* 558: 564–67.

Postberg, F., Schmidt, J., Hillier, J., Kempf, S., and Srama, R. 2011. A Salt-Water Reservoir as the Source of a Compositionally Stratified Plume on Enceladus. *Nature* 474: 620–22.

Postberg, F., Sekine, Y., Klenner, F., Glein, C. R., Zou, Z., Abel, B., Furuya, K., et al. 2023. Detection of Phosphates Originating from Enceladus's Ocean. *Nature* 618: 489–493. https://doi.org/10.1038/s41586-023-05987-9.

Price, M. C., Kearsley, A. T., and Burchell, M. J. 2013. Validation of the Preston-Tonks-Wallace Strength Model at Strain Rates of 10^{13} s^{-1} for Al-1100, Tantalum and Copper Using Hypervelocity Impact Crater Morphologies. *International Journal of Impact Engineering* 52: 1–10.

Price, M. C., Solscheid, C., Burchell, M. J., Josse, L., Adamek, N., and Cole, M. J. 2013. Survival of Yeast Spores in Hypervelocity Impact Events Upto Velocities of 7.4 km s^{-1}. *Icarus* 222: 263–272.

Ratcliff, P. R., Burchell, M. J., Cole, M. J., Murphy, T. W., and Allahdadi, F. 1997. Experimental Measurements for Hypervelocity Impact Plasma Yield and Energetics. *International Journal of Impact Engineering* 20: 663–674. https://doi.org/10.1016/S0734-743X(97)87453-2.

Reh, K., Spilker, J., Lunine, J. L., Waite, J. H., Cable, M., Postberg, F., and Clarke, K. 2016. Enceladus Life Finder: The Search for Life in a Habitable Moon, 2016 IEEE Aerospace Conference, Big Sky, MT, USA, pp. 1–8 https://doi.org/10.1109/AERO.2016.7500813.

Roth, L., Saur, J., Retherford, K. D., Strobel, D. F., Feldman, P. D., McGrath, M. A., and Nimmo, F. 2014. Transient Water Vapor at Europa's South Pole. *Science* 10: 171–74. https://doi.org/10.1126/science.1247051.

Rotundi, A., Sierks, H., Della Corte, V., Fulle, M., Gutierrez, P. J., Lara, L., Barbieri, C., et al. 2015. Dust Measurements in the Coma of Comet 67P/Churyumov-Gerasimenko in Bound to the Sun. *Science* 347: aaa3905. https://doi.org/10.1126/science.aaa3905.

Russel, R. P., and Lara, M. 2009. On the Design of an Enceladus Science Orbit. *Acta Astronautica* 65: 27–39. https://doi.org/10.1016/j.actaastro.2009.01.021.

Schenk, P., Clark, R. N., Howett, C. J. A., Verbiscer, A. J., and Waite, J. H. 2018. *Enceladus and the Icy Moons of Saturn*. Tucson, AZ: University of Arizona Press.

Singh, S. V., Dilip, H., Meka, J. K., Thiruvenkatam, V., Vishakantaiah, J., Muruganathan, M., Vijayan, S., et al. 2022. New Signatures of Bio-Molecular Complexity in the Hypervelocity Impact Ejecta of Icy Moon Analogues. *Life* 12: 508. https://doi.org/10.3390/life12040508.

Soderblom, L. A., Kieffer, S. W., Becker, T. L., Brown, R. H., Cook, A. F., Hansen, C. J., Johnson, T. V., Kirk, R. L., and Shoemaker, E. M. 1990. Triton's Geyser-like Plumes: Discovery and Basic Characterization. *Science* 250: 410–15.

Soderlund, K. M., Kalousová, K., Buffo, J. J., Glein, C. R., Goodman, J. C., Mitri, G., Patterson, G. W., et al. 2020. Ice-Ocean Exchange Processes in the Jovian and Saturnian Satellites. *Space Science Reviews* 216: 80. https://doi.org/10.1007/s11214-020-00706-6.

Southworth, B. S., Kempf, S., and Schmidt, J. 2015. Modeling Europa's Dust Plumes. *Geophysical Research Letters* 42: 10541–48. https://doi.org/10.1002/2015GL066502.

Southworth, B. S., Kempf, S., and Spitale, J. 2019. Surface Deposition of the Enceladus Plume and the Zenith Angle of Emissions. *Icarus* 319: 33–42. https://doi.org/10.1016/j.icarus.2018.08.024.

Spahn, F., Schmidt, J., Albers, N., Hörning, M., Makuch, M., Seiß, M., Kempf, S., et al. 2006. Cassini Dust Measurements at Enceladus and Implications for the Origin of the E Ring. *Science* 311: 1416–18.

Sparks, W. B., Hand, K. P., McGrath, M. A., Bergeron, E., Cracraft, M., and Deustua, S. E. 2016. Probing for Evidence of Plumes on Europa with HST/STIS. *The Astrophysical Journal* 829: 121.

Spencer, J. R., Nimmo, F., Ingersoll, A. P., Hurford, T. A., Kite, E. S., Rhoden, A. R., Schmidt, J., and Howett, C. J. A. 2018. Plume Origins and Plumbing (Ocean to Surface). In *Enceladus and the Icy Moons of Saturn*, edited by P. M. Schenk, R. N. Clark, C. J. A. Howett, J. A. Verbiscer, and J. H. Waite, 163–174. Tucson, AZ: University of Arizona. https://doi.org/10.2458/azu_uapress_9780816537075-ch008.

Srama, R., Ahrens, T. J., Altobelli, N., Auer, S., Bradley, J. G., Burton, M., Dikarev, V. V., et al. 2004. The Cassini Cosmic Dust Analyzer. *Space Science Reviews* 114: 465–518.

Srama, R., Woiwode, W., Postberg, F., Armes, S. P., Fujii, S., Dupin, D., Ormond-Prout, J., et al. 2009. Mass Spectrometry of Hyper-Velocity Impacts of Organic Micrograins. *Rapid Communications in Mass Spectrometry* 23: 3895–3906. https://doi.org/10.1002/rcm.4318.

Stern, S. A., Bagenal, F., Ennico, K., Gladstone, G. R., Grundy, W. M., McKinnon, W. B., Moore, J. M., et al. 2015. The Pluto System: Initial Results from its Exploration by New Horizons. *Science* 350: aad1815. https://doi.org/10.1126/science.aad1815.

Stern, S. A., Grundy, W. M., McKinnon, W. B., Weaver, H. A., and Young, L. A. 2018. The Pluto System After New Horizons. *Annual Review of Astronomy and Astrophysics* 56: 357–392. https://doi.org/10.1146/annurev-astro-081817-051935.

Sugahara, H., and Mimura, K. 2015. Peptide Synthesis Triggered by Comet Impacts: A Possible Method for Peptide Delivery to the Early Earth and Icy Satellites. *Icarus* 257: 103–112.

Takeuchi, Y., Furukawa, Y., Kobayashi, T., Sekine, T., Terada, N., and Kakegawa, T. 2020. Impact-Induced Amino Acid Formation on Hadean Earth and Noachian Mars. *Scientific Reports* 10: 9220.

Taubner, R.-S., Olsson-Francis, K., Vance, S. D., Ramkissoon, N. K., Postberg, F., de Vera, J. P., Antunes, A., et al. 2020. Experimental and Simulation Efforts in the Astrobiological Exploration of Exooceans. *Space Science Reviews* 216: 41. https://doi.org/10.1007/s11214-020-0635-5.

Thomas, P. C., Tajeddine, R., Tiscareno, M. S., Burns, J. A., Joseph, J., Loredo, T. J., Helfenstein, P., and Porco, C. 2016. Enceladus's Measured Physical Libration Requires a Global Subsurface Ocean. *Icarus* 264: 37–47. https://doi.org/10.1016/j.icarus.2015.08.037.

Traspas, A., and Burchell, M. J. 2021. Tardigrade Survival Limits in High Speed Impacts—Implications for Panspermia and Collection of Samples from Plumes Emitted by Ice Worlds. *Astrobiology* 21: 845–852. https://doi.org/10.1089/ast.2020.2405.

Trigo-Rodríguez, J. M., Domínguez, G., Burchell, M., Hörz, F., and Llorca, J. 2009. Bulbous Tracks Arising from Hypervelocity Capture in Aerogel. *Meteoritics & Planetary Science* 43: 75–86.

Tsou, P., Brownlee, D. E., McKay, C. E., Anbar, A. D., Yano, H., Altwegg, K., Beegle, L. W., Dissly, R., Strange, N. J., and Kanik, I. 2012. LIFE: LIFE Investigation for Enceladus A Sample Return Mission Concept in Search for Evidence of LIFE. *Astrobiology* 12: 730–742.

Tsou, P., Brownlee, D. E., Sandford, S. A., Hörz, F., and Zolensky, M. E. 2003. Wild 2 and Interstellar Sample Collection and Earth Return. *Journal of Geophysical Research* 108: 8113.

Vance, S., Harnmeijer, J., Kimura, J., Hussman, H., de Martin, B., and Brown, J. M. 2007. Hydrothermal Systems in Small Ocean Planets. *Astrobiology* 7: 987–1005. https://doi.org/10.1089/ast.2007.0075.

Waite, J. H., Combi, M. R., Ip, W. H., Cravens, T. E., McNutt, R. L., Kasprzak, W., Yelle, R., et al. 2006. Cassini Ion and Neutral Mass Spectrometer: Enceladus Plume Composition and Structure. *Science* 311: 1419–22.

Westphal, A. J., Stroud, R. M., Bechtel, H. A., Brenker, F. E., Butterworth, A. L., Flynn, G. J., Frank, D. R., et al. 2014. Laboratory Identification of Probable Interstellar Dust Particles Collected by the Stardust Spacecraft. *Science* 345: 786–791. https://doi.org/10.1126/science.1252496.

Wozniakiewicz, P. J., Bridges, J., Burchell, M. J., Carey, W., Carpenter, J., Della Corte, V., Dignam, A., et al. 2021. A Cosmic Dust Detection Suite for the Deep Space Gateway. *Advances in Space Research* 68: 85–104.

Wozniakiewicz, P. J., Ishii, H. A., Kearsley, A. T., Burchell, M. J., Bradley, J. P., Price, M. C., Teslich, N., Lee, M. R., and Cole, M. J. 2012. Stardust Impact Analogs: Resolving Pre- and Post-Impact Mineralogy in Stardust Al Foils. *Meteoritics & Planetary Science* 47: 708–728.

Wozniakiewicz, P. J., Kearsley, A. T., Burchell, M. J., Price, M. C., Ishii, H., and Cole, M. J. 2018. Preparation of Large Stardust Aluminum Foil Craters for Analysis. *Meteoritics & Planetary Science* 53: 1066–80.

Wozniakiewicz, P. J., Price, M. C., Armes, S. P., Burchell, M. J., Cole, M. J., Fielding, L. A., Hillier, J. K., and Lovett, J. R. 2014. Micron-Scale Hypervelocity Impact Craters: Dependence of Crater Ellipiticity on Impact Trajectory, Projectile Size, Velocity and Shape. *Meteoritics & Planetary Science* 49: 1929–47. https://doi.org/10.1111/maps.12364.

Yamagishi, A., Yokobori, S., Kobayashi, K., Mita, H., Yabuta, H., Tabata, M., Higashide, M., and Yano, H. 2021. Scientific Targets of Tanpopo: Astrobiology Exposure and Micrometeoroid Capture Experiments at the Japanese Experiment Module Exposed Facility of the International Space Station. *Astrobiology* 12: 1451–60.

Yano, H., Arakawa, M., Michikami, T., and Fujiwara, A. 1999. Sub-Millimeter-Sized Ice Grain Impacts on Aerogels: Implications to a Cometary Dust Sample Return Mission. 30th Lunar and Planetary Science Conference, abstract #1961.

Zimmer, C., Khurana, K. K., and Kivelson, M. G. 2000. Subsurface Oceans on Europa and Callisto: Constraints from Galileo Magnetometer Observations. *Icarus* 147: 329–347. https://doi.org/10.1006/icar.2000.6456.

APPENDIX 1
ORBITAL PERIOD VERSUS ALTITUDE

Consider the simple case of an unpowered, gravitationally bound circular orbit of a body mass M. By equating the force due to gravity with that needed for centripetal motion, we obtain:

$$v = \sqrt{[GM/r_a]}, \tag{A1}$$

where G is the gravitational constant, and r_a is the radius of the orbit. For motion in a circle, the speed can also be expressed as.

$$v = 2\pi r_a/P, \tag{A2}$$

where P is the period. Thus we obtain:

$$P = \sqrt{\left[4\pi^2 {r_a}^3/\mathrm{GM}\right]}. \tag{A3}$$

We can also write that.

$$M = 4/3\pi r^3\rho, \tag{A4}$$

where r is the radius of the body and ρ its mean density. We thus find.

$$P = \sqrt{\left[3\pi {r_a}^3/G\rho r^3\right]}. \tag{A5}$$

If we note that $r_a = r + a$, where a is altitude, we can write:

$$P = \sqrt{\left[\left(3\pi/G\rho r^3\right) \times (r+a)^3\right]}. \tag{A6}$$

Expanding $(r + a)3$ as $r^3\{1 + 3a/r + 3(a/r)^2 + (a/r)^3\}$, allows us to write:

$$P = \sqrt{\left[\left(3\pi/G\rho r^3\right) \times r^3\left\{1 + 3a/r + 3(a/r)^2 + (a/r)^3\right\}\right]}, \tag{A7}$$

which simplifies to:

$$P = \sqrt{\left[(3\pi/G\rho)\left\{1 + 3a/r + 3(a/r)^2 + (a/r)^3\right\}\right]}. \tag{A8}$$

We can now consider various limiting cases. In the case that ρ is the same for all bodies of interest, then $3\pi/G\rho$ is effectively a constant, so orbital period only varies with the ratio a/r to power 1–3.

In addition, if all such bodies were of similar size, then orbital periods on these worlds are all similar as a function of altitude.

We can go further if the altitude a is small compared to the radius of the body r, then a/r can be neglected, and $P \to \sqrt{[3\pi/G\rho]}$. The same result applies if a itself is vanishingly small or r tends to infinity. In such cases, P only depends on ρ.

Thus, for bodies of similar density, the orbital period converges to the same value at very low altitudes, or at low to moderate altitudes if the body has a large radius.